Contrasting impacts of forest on cloud cover based on satellite observations

Ru Xu[1,2], Yan Li[1,2*], Adriaan J. Teuling[3], Lei Zhao[4,5], Dominick V. Spracklen[6], Luis Garcia-Carreras[7], Ronny Meier[8], Liang Chen[9], Youtong Zheng[10], Bojie Fu[1,11]

1. State Key Laboratory of Earth Surface Processes and Resources Ecology, Beijing Normal University, Beijing 100875, China

2. Institute of Land Surface System and Sustainable Development, Faculty of Geographical Science, Beijing Normal University, Beijing 100875, China

3. Hydrology and Quantitative Water Management Group, Wageningen University and Research, Wageningen, The Netherlands.

4. Department of Civil & Environmental Engineering, University of Illinois at Urbana-Champaign, Urbana, IL 61801, USA.

5. National Center for Supercomputing Applications, University of Illinois at Urbana-Champaign, Urbana, IL 61801, USA.

6. School of Earth and Environment, University of Leeds, Leeds, LS2 9JT, UK

7. Centre for Atmospheric Science, Department of Earth and Environmental Sciences, University of Manchester, Manchester, M139PL, United Kingdom

8. Institute for Atmospheric and Climate Science, ETH Zurich, 8092 Zurich, Switzerland

9. Climate and Atmospheric Sciences Section, Illinois State Water Survey, Prairie Research Institute, University of Illinois at Urbana-Champaign, Champaign, IL 61820 USA

10. Earth System Science Interdisciplinary Center, University of Maryland, College Park, Maryland, 20742, USA.

11. State Key Laboratory of Urban and Regional Ecology, Research Center for Eco-Environmental Sciences, Chinese Academy of Sciences, Beijing, 100085, China

*Correspondence Yan Li: yanli.geo@gmail.com

Abstract:

Forests play a pivotal role in regulating climate and sustaining the hydrological cycle. The biophysical impacts of forest on clouds, however, remain unclear due to the lack of direct observations. In this first global-scale observational study, we use long-term satellite-derived cloud cover data to show that forests can have opposite effects on summer cloud cover. We find enhanced cloud cover over most temperate and boreal forests, but inhibited cloud cover over Amazon, central Africa, and Southeast US. These cloud effects mainly arise from convection processes associated with forests. The spatial variation in the sign of cloud effects is driven by sensible heating where cloud enhancement (inhibition) is more likely to occur when sensible heat in forest is larger (smaller) than nearby nonforest. Ongoing forest cover loss has led to opposite cloud cover changes, with local cloud increase over forest loss hotspots in the Amazon (+0.78%), Indonesia (+1.19%), and Southeast US (+0.09%), but cloud reduction in East Siberia (-0.20%) from 2002-2018. Our data-driven assessment informs the climate effects of local-scale forest cover change and improves mechanistic understanding of forest-cloud interactions, the latter of which remains uncertain in Earth system models.

Introduction

Forests regulate climate and sustain the hydrological cycle through biophysical processese[1,2]. These processes are tightly linked to land surface properties, such as albedo, roughness, and canopy conductance that affect the exchange of energy and water between the land and atmosphere[1,2]. The direct biophysical impacts of forest on surface temperature have been extensively studied, revealing a latitudinal transition from tropical cooling to boreal warming[3–5]. However, less attention has been paid to its indirect impacts on clouds and precipitation, two physically linked key components in the hydrological cycle. How clouds and precipitation respond to land cover change has been poorly constrained and presents one of the major challenges in climate change assessment[6].

Global climate models (GCMs) have predicted a reduction in precipitation and a frequent decrease in cloud cover resulting from large-scale deforestation, with the greatest decrease in tropical regions[7–9]. Although these results are in line with the common perception that vegetation enhances clouds and precipitation[10], these continental- or global-scale land clearing experiments implemented in models with a relatively coarse resolution are not consistent with the ongoing small-scale land activities in the real world. Results from these GCM experiments are often complicated by mixing the local-scale intrinsic biophysical mechanism with the nonlocal feedbacks triggered by large-scale land cover change in the climate system, making it hardly comparable with observations[11,12].

In contrast to cloud and precipitation reduction simulated in the GCM experiments[7,8,13], high-resolution regional climate models[14,15] and empirical analyses using satellite imagery [16,17] reported that small-scale deforestation increases rather than decreases clouds and precipitation in Amazon due to land surface heterogeneity[18]. These results revealed inhibited clouds over forest (e.g., West Africa[19]) at a realistic scale which seemingly contradicts the highly hypothetical GCM results[20] and enhanced cloud observations over forest in other regions (e.g., western Europe[21] and Central America[22]).

These inconsistent findings among modeling and observational studies highlight the large uncertainty in cloud and convection representations in climate models [23,24] as well as the complexity of forest–cloud interactions, which involve different mechanisms across different scales with varying regional importance[25]. The global pattern of forest impacts on cloud cover, and how it is shaped by the interplay of different mechanisms remain largely unresolved. In this study, we use satellite observations of high spatial resolution and long-term global coverage to assess the cloud effect of forests across the globe, exploring the possible mechanisms with data-driven approaches, and to quantify the cloud effects of forest loss in the recent two decades.

Results

Potential effects of forest on cloud cover

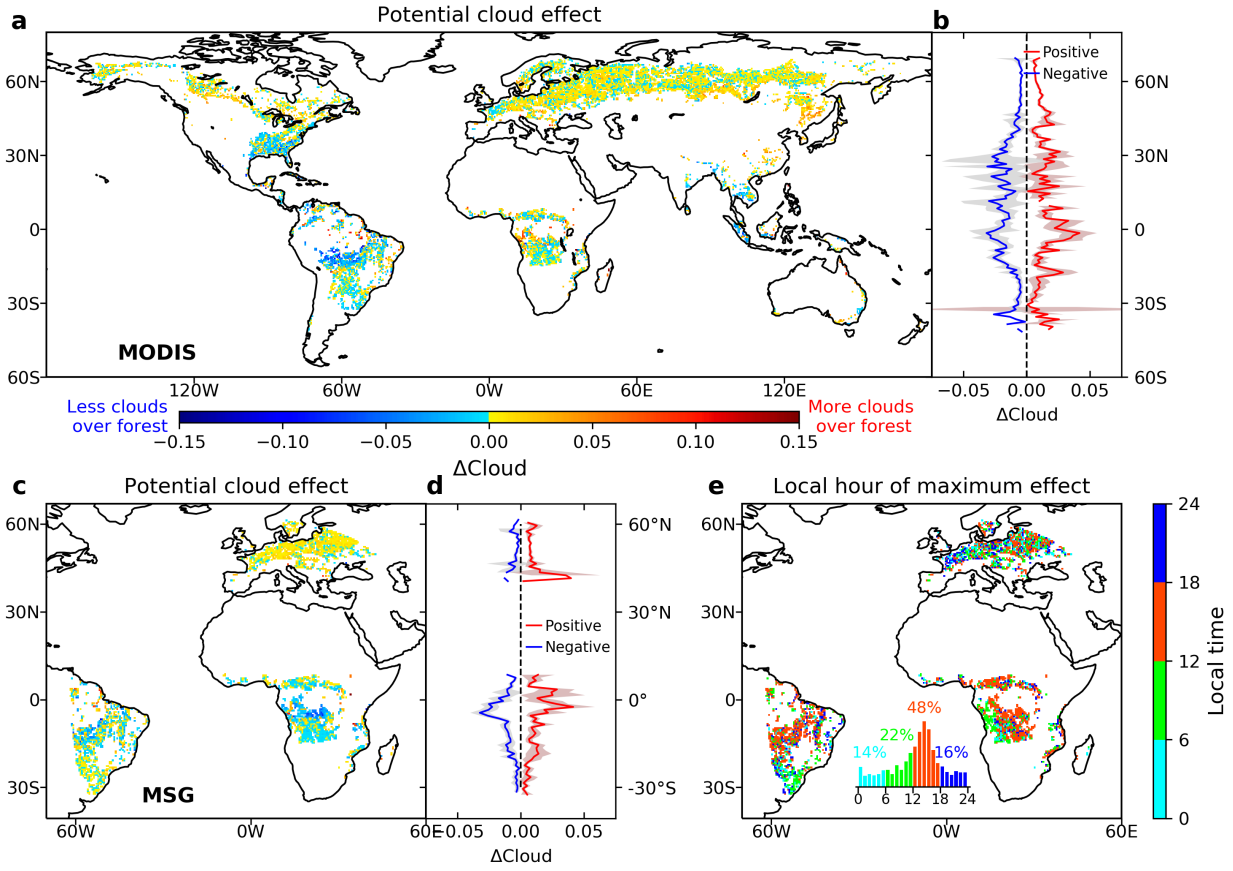

Figure 1. Potential effects of forest on June-August (JJA) cloud cover. Potential effect is defined as the cloud differences of forest minus nonforest (ΔCloud). (a) Potential effects of forest on cloud cover based on MODIS data from 2002 to 2018 (overpass at 13:30 local time) and (b) their latitudinal pattern. (c,d) Potential effects of forest on cloud cover based on hourly MSG data from 2004 to 2013 (overpass at 14:00 local time) and (e) timing of the maximum effect during a day.

Using a space-for-time approach, we define the potential cloud effect of forest as the multiyear mean cloud difference between unchanged forest and nearby nonforest pixels ($\Delta Cloud = Cloud_{forest} - Cloud_{nonforest}$). The positive and negative ΔCloud denote (spatial) enhanced and inhibited cloud cover over forest, respectively. ΔCloud is estimated globally through a 9 by 9 cell moving window (0.45 × 0.45°) near locations that underwent forest cover change during the study period (see methods). This approach is able to minimize cloud effects resulting from large-scale circulation/climate changes which affect both forest and nonforest. The climatological approach also effectively removes stochastic cloud differences

between forest and nonforest caused by individual meteorological events and wind direction changes. Here we primarily focus on boreal summer months (JJA) which maximize the cloud differences between forest and nonforest[21], while results for other seasons are provided in the supplementary information.

Forest exhibits a regionally varying effect on JJA cloud cover based on MODIS data (overpass at 13:30 local time, Fig. 1a). Most temperate and boreal forests in Eurasia and North America, accounting for 63.21% of the grid boxes, show a cloud enhancement effect (positive ΔCloud, +0.0133 on average). In contrast, forests in South Amazon, Central Africa, and Southeast US show a cloud inhibition effect (negative ΔCloud, -0.0115 on average). These cloud effects follow a latitudinal dependency with the largest effect in the tropical regions, likely due to strong turbulence fluxes contrast between forest and nonforest at low latitudes which is preferential for convection development. The cloud effects are diminished toward higher latitudes, regardless of sign (Fig. 1b). Our additional sensitivity tests indicate that the global pattern of ΔCloud still holds when estimated using alternative window sizes (see methods, Fig. S1) and splitted time periods (2002-2007, 2008-2013, 2014-2018, Fig. S2), suggesting the robustness of results to scale of local window and interannual variability of cloud cover.

Similar spatial and latitudinal patterns can be seen from MSG data (at 14:00 local time), with cloud inhibition being stronger in central Africa while weaker in the Amazon regions, despite reduced spatial coverage (Fig. 1c,d). The hourly resolution of MSG cloud data reveals a pronounced diurnal cycle in the cloud effect (Figs. 1e, S3). Consistent with the daytime prevalence of convection, the maximum effect during the course of the day (the largest ΔCloud regardless of sign) occurs mostly at daytime (6AM to 18PM, 70%), especially during afternoon (12 to 18PM, 48%) in tropical regions.

The MODIS and MSG cloud cover data provide a combined measure of cloud fraction but they do not separate different cloud types. By utilizing Sentinel-5P cloud data and a cloud classification scheme[26], we are able to estimate cloud effects of forest with respect to different cloud types (see methods). We find that globally, cloud effects are dominated by convective clouds in 45.01% of grid boxes, largely contributed by shallow convective stratocumulus clouds (39.10%) (Fig. S4). Regionally, the convection dominance becomes more prominent, contributing to 68.13% of cloud effects in the Amazon. These

further confirm that cloud effects of forests shown in our study are primarily convection-driven, as also implied by MODIS and MSG data.

In terms of seasonality, there are notable and region-specific variations in ΔCloud from MODIS data (Figs. S5, S6). In tropical forests, cloud inhibition is stronger during the dry season in the Amazon, whereas it is amplified during the wet season in Central Africa. In temperate forests, cloud inhibition in the Southeast US is larger in summer, while cloud enhancement in Europe is relatively stable during the snow-free period.

Attribution of cloud effects of forest

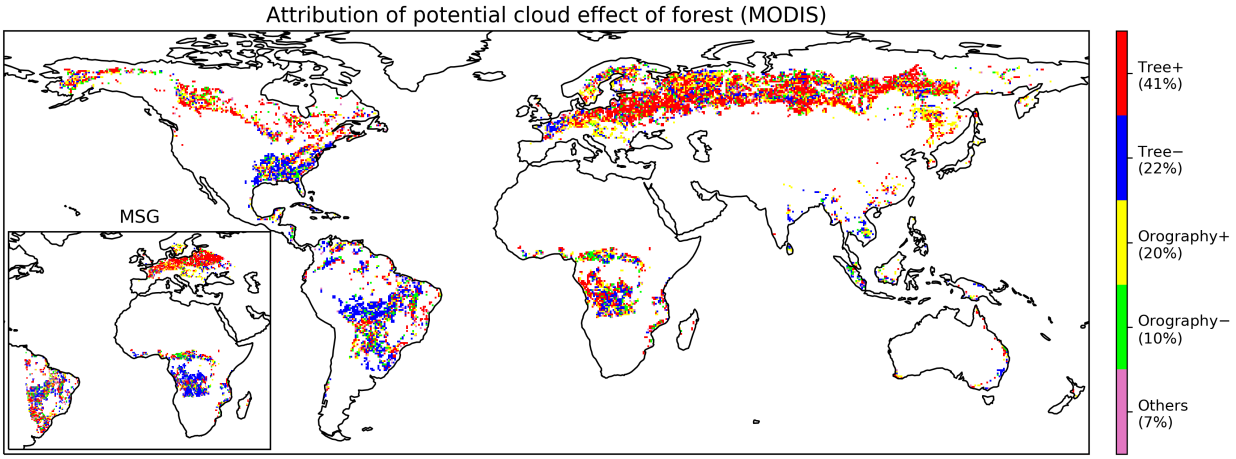

Figure 2. Attribution of cloud effects of forest to tree cover and elevation based on MODIS and MSG data. The five attribution categories include tree cover induced cloud increase (Tree+) and decrease (Tree-), orography induced cloud increase (Orography+) and decrease (Orography-), and other unexplained effects.

Estimating the cloud effect of forest could be confounded by orographic clouds because of the dual influences of topography on forest distribution and cloud formation. Forest tends to be located at a higher elevation and in more complex terrain than nonforest[27]. Although regions with complex topography are masked out in our analysis (see methods), the high elevation of forest *per se* could facilitate cloud formation through orographic lifting of moist air[28], leading to increased cloud cover over forest (Fig. S7).

To address this issue, we decompose ΔCloud into contributions of tree cover and elevation (see

methods, Fig. S8). The attribution shows that the global pattern of ΔCloud is dominated by tree cover induced cloud effects (41% grid boxes for cloud enhancement and 22% for cloud inhibition), followed by elevation induced cloud effects (30%), and unexplained effects due to other factors (7%) (Fig. 2). This confirms that most of the observed cloud effects are robust features attributable to tree cover rather than topography and other factors.

The mechanisms of contrasting cloud effects of forest

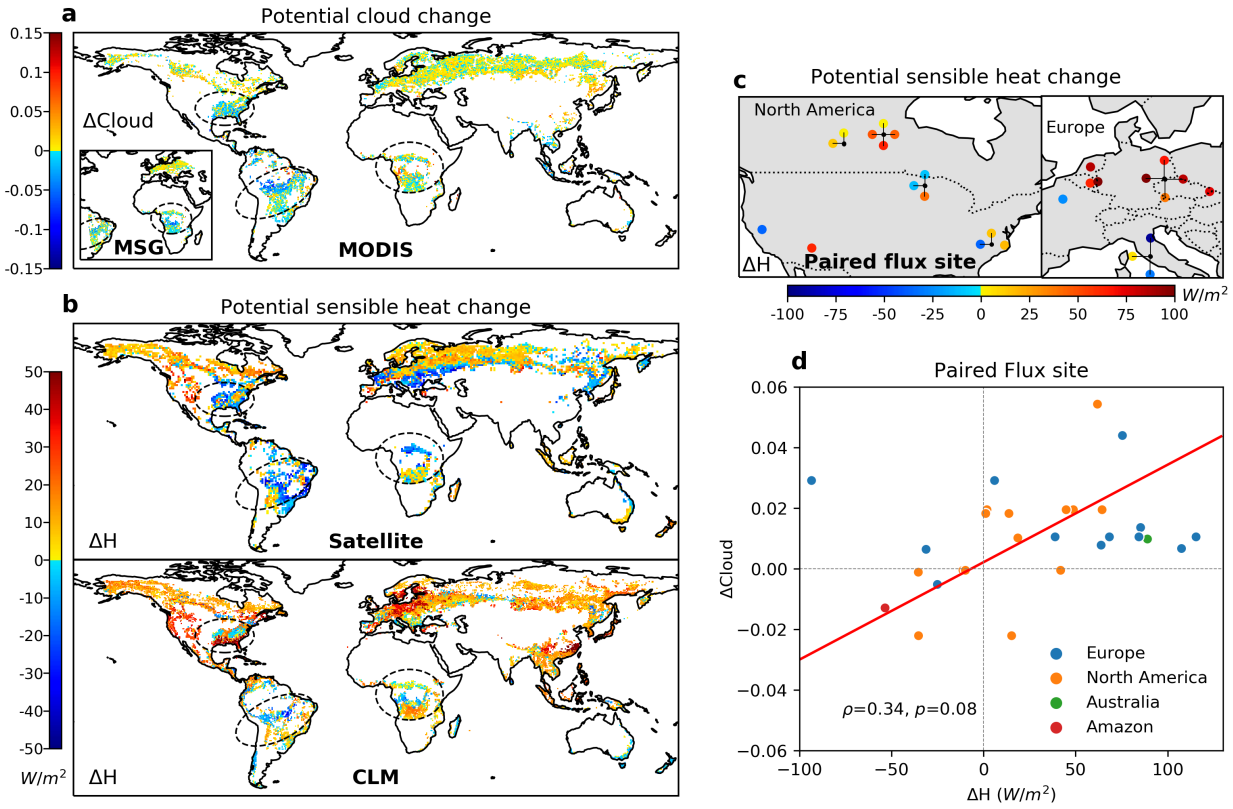

Figure 3. Potential effect of forest on sensible heat and its relationship with cloud effect of forest. (a) Potential effect of forest on cloud cover from MODIS and MSG data (duplicated from Fig 1a,b). (b) Potential effect of forest on sensible heat (ΔH) estimated from satellite data[4], CLM5, and (c) 28 paired forest and nonforest flux sites. The connection lines in panel (c) indicate the location of flux tower clusters and one pair in the Amazon is not shown on the map. (d) The relationship between potential effect of forest on sensible heat and on cloud cover (ΔCloud) at paired flux towers. The cloud effects at

paired flux sites location are extracted from ΔCloud aggregated to 1° based on MODIS data. The fitted line is estimated by geometric mean regression[29]. The spearman's correlation coefficient (ρ) and its p-value (p) are shown at the bottom.

While different biophysical processes are involved in the forest-cloud interaction, it is still unclear which factors determine the spatial occurrences of cloud enhancement and inhibition over different forests. The geographic variations in specific land cover types of global forest and nonforest vegetation show little spatial resemblance to ΔCloud (Fig. S9). In terms of biophysical differences, forest has reduced albedo, higher roughness, lower land surface temperature (LST), increased evapotranspiration and soil moisture than nonforest vegetation[4,5]. However, these differences are common to almost all forests and are unable to explain the contrasting cloud effects, as indicated by their mismatched spatial patterns with ΔCloud (Fig. S10).

We find that the sensible heat difference between forest and nonforest (ΔH) is an effective differentiator for the sign of cloud effect among other land surface properties[30]. This is obtained by analyzing the relationship between ΔCloud and ΔH derived from three independent datasets based on satellite[4], simulation of Community Land Model (CLM) version 5[31], and 28 paired forest and nonforest flux sites[32](Fig. 3a-c). Both satellite and CLM data indicate that cloud inhibition (negative ΔCloud) mainly occurs at locations where forests exhibit a smaller sensible heat flux than nonforest (negative ΔH), including southern Amazon[33], central Africa, and the southeast US (three circles in Fig. 3a,b). By contrast, cloud enhancement (positive ΔCloud) in the rest of the world broadly corresponds to locations with higher sensible heating in forest (positive ΔH), despite few inconsistencies in southern Europe among the considered datasets. Such a spatial co-occurrence is further confirmed by the positive relationship between ΔH from paired flux sites and ΔCloud (Fig. 3d), suggesting that cloud enhancement (inhibition) is more likely to occur when forests have higher (smaller) sensible heat flux than nonforest .

The spatial patterns of ΔH reflect the biophysical and climatic controls on energy redistribution in forest and nonforest along latitude and moisture levelsl[34,35]. The small Bowen ratio in forest at low latitude under humid climates channels most available energy into latent heat rather than sensible heat, resulting

169 in even smaller sensible heat compared to nonforest, while the large Bowen ratio at higher latitudes under
170 drier climates leads to the opposite effect. The collective evidence demonstrates the central role of
171 sensible heat in convection triggering and cloud formation[30]. The higher sensible heat relative to nearby
172 land is indicative of a preferable condition for convection and cloud development, though it is caused by
173 different mechanisms for enhanced and inhibited cloud cover over forest, respectively.
174

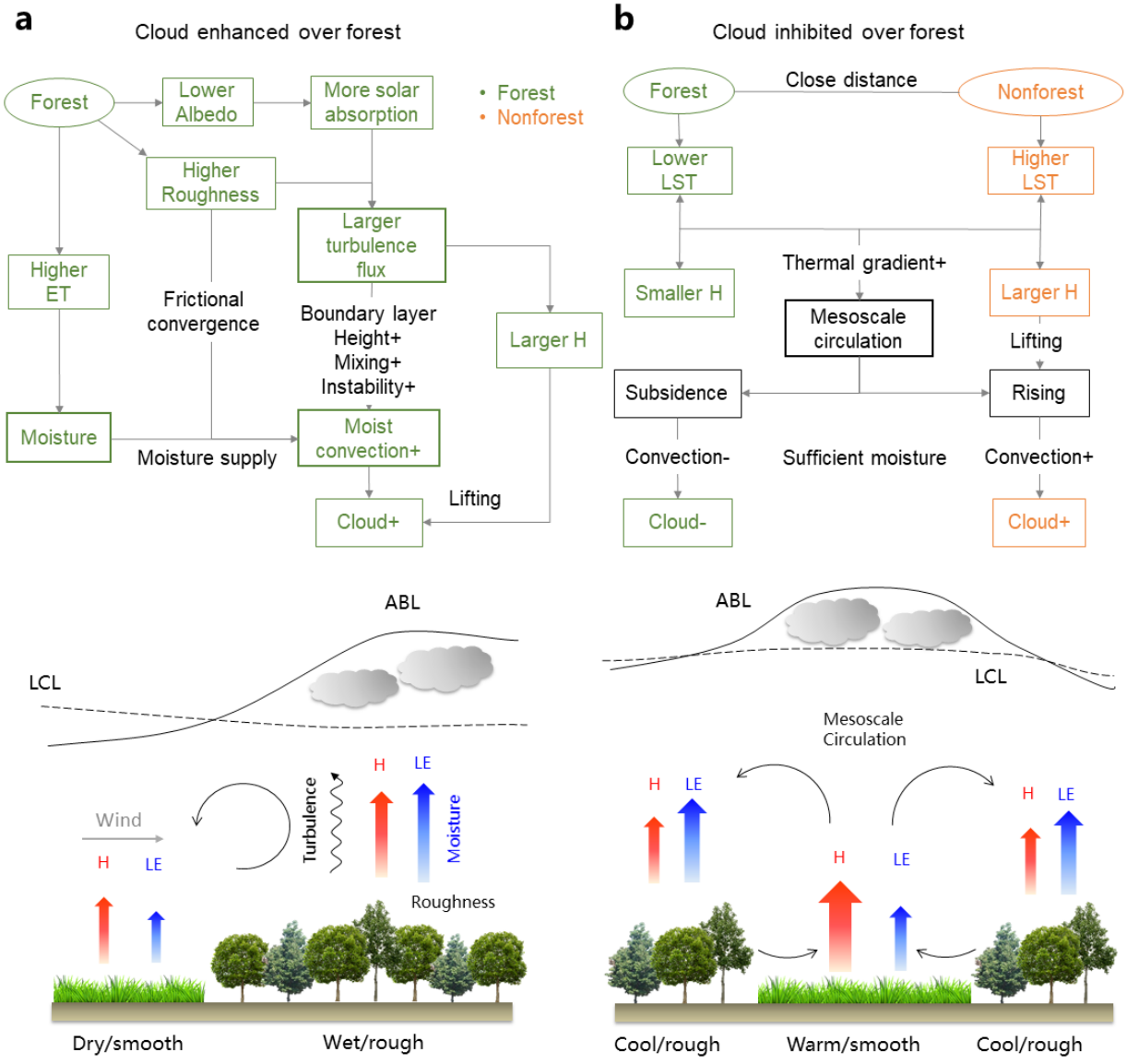

175

176 Figure 4. Mechanisms of contrasting cloud effects of forests. (a) Clouds enhanced over forest through
177 increased convection due to increased moisture supply and turbulence. (b) Clouds inhibited over forest

through suppressed convection due to divergence of mesoscale circulations. ABL: atmospheric boundary layer. LCL: lifting condensation level. LE: latent heat. H: sensible heat.

The mechanisms of enhanced cloud over forest are associated with several interconnected processes conducive to the growth of moist convection (Fig. 4a). Compared with nonforest vegetation, forest usually exhibits high evapotranspiration[5], which provides abundant water vapor supply for cloud formation and sustains moisture recycling[36,37]. The low albedo and high roughness of forest promote a greater fraction of incoming solar energy to be partitioned into turbulent fluxes, increasing turbulent mixing and convective instability in the boundary layer[15,38,39]. The differential roughness between forest and nonforest induces frictional convergence in downwind direction[21,40]. Enhanced sensible heating, which typically occurs in forest relative to nonforest vegetation[32], serves as a major lifting mechanism to initiate convection and the growth of boundary layer[30,38].

The mechanisms of inhibited cloud cover over forest and enhanced cloud cover over nearby nonforest, are linked to the mesoscale circulation triggered by heat and moisture anomalies of heterogeneous landscape between forest and nonforest[41] (Fig. 4b). Differential heating between forest (cooler) and nonforest (warmer) creates a thermally-driven mesoscale circulation analogous to a sea-breeze. The rising airflow over nonforest initiates convective clouds while the subsidence branch over forest outweighs moist convection processes and inhibits cloud development. The warmer deforested areas with larger sensible heat flux, combined with increased atmospheric instability[15] can reinforce mesoscale circulation and provide a favorable environment for cloud formation[14,38,42].

The development of mesoscale circulation also depends on the length scale of the land heterogeneity and synoptic conditions. Mesoscale circulation is typically generated at spatial scales of 10~100km[15,39] and gets intensified under weak synoptic conditions (e.g., stronger cloud inhibition in Amazon in the dry season when synoptic winds are weaker and LST gradient is larger)[5,14,17]. To investigate the sensitivity of cloud inhibition induced by mesoscale circulation to spatial scale, we re-estimated ΔCloud using MODIS cloud data resampled to different spatial resolutions. We find that with reduced resolutions of cloud data, the spatial coverage of cloud inhibition shrinks from ~37% at 0.05° to

~24~28% at 1°, while cloud enhancement becomes more dominant (from 63% to ~76~72%) (Fig. S11, Tab. S3). This implies that at coarser scales, at which mesoscale processes become less important (i.e., less cloud inhibition), observation- and model-based results tend to converge on cloud enhancement of forest.

Cloud effects of forest loss in recent two decades

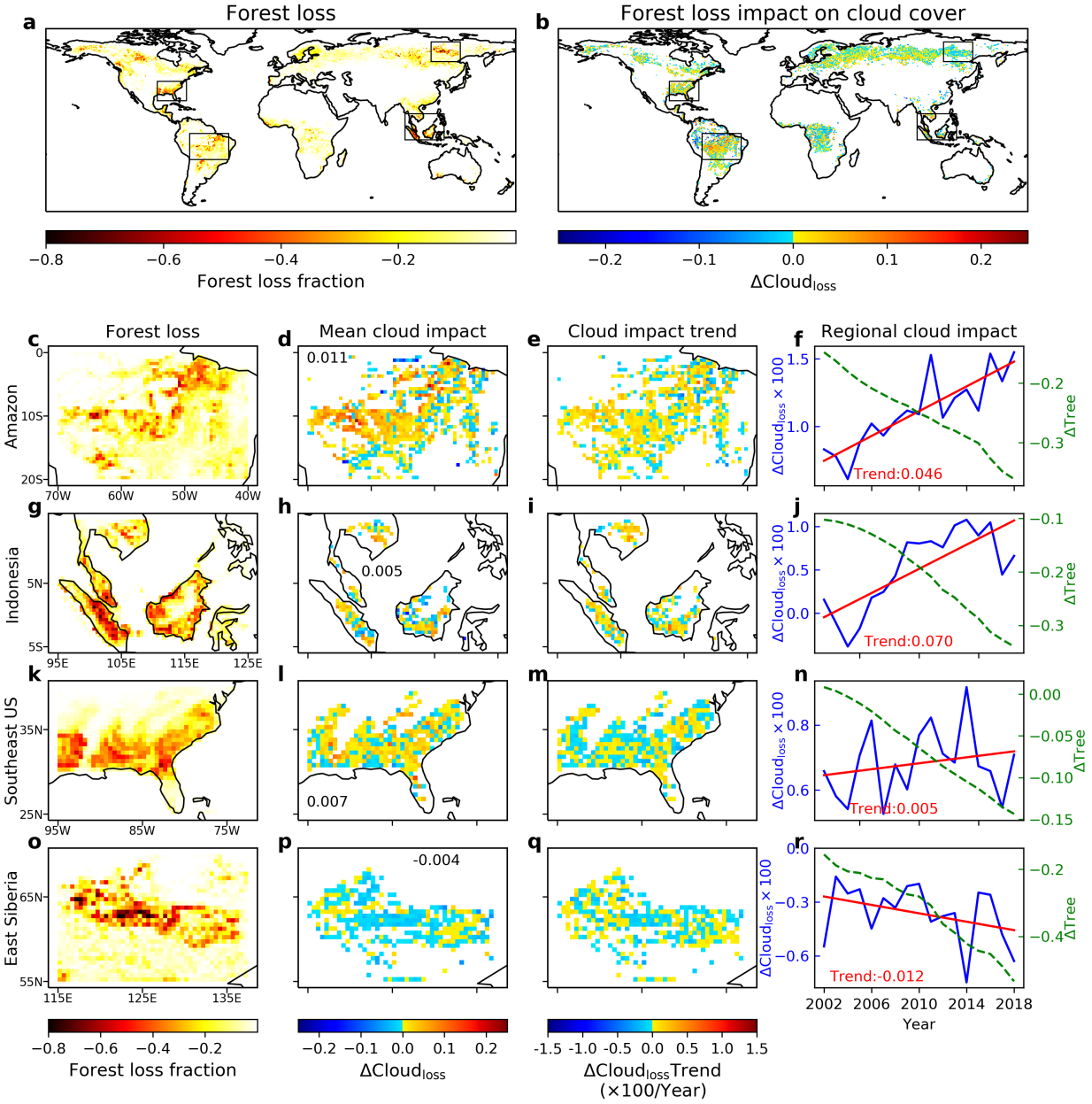

Figure 5. Impacts of forest loss on JJA cloud cover based on MODIS data from 2002 to 2018. (a) The accumulated forest loss fraction from 2001 to 2018 and (b) the actual impact of forest loss ($\Delta Cloud_{loss}$), defined as the mean cloud difference between forest loss location and unchanged forest from 2002 to 2018. Four hotspots (Amazon, Indonesia, East Siberia, and Southeast US, row-wise), which experienced intensive forest loss are highlighted in panels c to r, including their forest loss fractions, mean $\Delta Cloud_{loss}$ during the study period, and regional and temporal trends of $\Delta Cloud_{loss}$ between 2002 and 2018 (column-wise). Green dashed line in the last column (f,j,n,r) shows tree cover difference between forest loss location and forest (ΔTree). Note that the cloud impacts in selected hotspot regions are estimated from grid boxes with tree cover loss fraction > 0.05. The unit of Trend (in red) is %/year in the last column.

Forest cover loss is rapidly occurring globally in recent two decades, especially in tropical regions owing to continuous deforestation (Fig. 5a)[43,44]. These changes are expected to cause different cloud responses in forests with enhanced or inhibited cloud effects. We quantify the actual cloud impact of forest loss that has already occurred by comparing cloud fraction at locations that underwent net loss in tree cover with nearby unchanged forest since 2000 (Fig. 5b) in four hotspot regions of forest loss (Fig. 5c,g,k,o).

During the study period, forest loss enhanced cloud cover in three of those hotspot regions: Amazon, Indonesia, and Southeast US, with mean cloud cover at forest loss location (tree cover loss >0.05) on average 0.011, 0.005, and 0.007 higher than nearby unchanged forest, respectively (Fig. 5 2nd column). Furthermore, enhanced cloud cover in these hotspots became increasingly stronger with the declining and more fragmented tree covert[45], which translates into total cloud fraction increases of 0.78% (0.046%/year), 1.19% (0.070%/year), and 0.09% (0.005%/year) over the course of 17 years (2002 to 2018) (3rd and 4th column in Fig. 5). Note that in the Amazon, forest loss legacy before 2001 had already caused increased cloud cover (positive ΔCloud) at the beginning of the study period (Fig. 5f). However, the presence of enhanced clouds over deforested regions requires the retaining of nearby forest patches over which clouds are reduced. As the scale of deforestation increases with fewer forest patches left, the mesoscale circulation induced cloud enhancement over deforested locations will decrease and ultimately

transit to a cloud reduction regime[13,42,46]. Unlike other hotspots, East Siberia is a region where forest loss induced cloud cover reduction. The mean cloud cover is 0.004 lower over the forest loss location than nearby unchanged forest (Fig. 5p). The cloud reduction also exhibited a strengthening trend, resulting in a total reduction in cloud cover fraction of -0.20% (-0.012%/year) from 2002 to 2018 (Fig. 5q, r). These results provide strong evidence that ongoing forest loss could emerge as an important driver for local cloud cover change, especially over areas with intensive forest loss.

Discussion

This study offers the first global-scale observational evidence for contrasting cloud effects of forest and advances our mechanistic understanding of the forest and cloud interaction. The cloud effect estimated in our study reflects the local impact of forest on cloud cover and is, therefore, more representative of real-world small-scale forest cover change, without generating the large-scale climate feedbacks which are usually triggered in GCM experiments[3,11]. The local perspectives allow us to identify the role of mesoscale circulation which is limited to small scales, a feature that has not been resolved by global climate models and is likely the cause of the discrepancy in clouds and precipitation response between climate model and observational studies, as also shown for soil moisture[24]. Although cloud processes are far more complicated than what is reflected in the cloud cover observation, our analysis provides a first-order approximation and benchmark for the forest and cloud interaction at fine-scale. These results can help constrain convection and cloud processes in climate models which are often parameterized and subject to large uncertainty.

Given the tight coupling of cloud and precipitation processes, the cloud impact of forest cover change may translate into precipitation[47]. Observational evidence exists in Amazon where the cloud increase in deforested areas has been accompanied by precipitation increase[48,49]. Although it is hard to directly detect precipitation impact of deforestation from observation[8], the cloud impact derived from high-resolution satellite data could provide useful inference to potential precipitation change, especially in tropical regions where convective rainfall is dominant[50]. However, distinct roles of different cloud types

(e.g., shallow cumulus clouds or deep convective clouds) in precipitation and radiative processes further complicate the inference from clouds to precipitation changes. Therefore, the extent to which forest loss induced cloud change translates to precipitation may depend on the region-, season-, and cloud type-specific cloud-precipitation interactions and requires further investigation.

Our results show ongoing forest cover loss has become an important driver of local cloud change over areas with intensive forest loss, which could potentially modify precipitation patterns and in turn, impose additional feedbacks to (either amplify or dampen) temperature change. Retaining forest patches could enhance cloud cover over nearby agricultural lands through mesoscale circulation (e.g., in Amazon) - with positive benefits of reduced temperature and possibly increased rainfall. Conversely, the reduction in cloud cover over remaining forest patches may reduce the resilience of the forest to future climate change[51]. Moreover, the changing forest cover owing to either deforestation or increased tree vulnerability under future warming[52,53] will not only affect local climate and hydrology, but could also have remote impacts on distant regions through moisture recycling and transportation[54] and other ecological and social-economic implications[55]. An accurate prediction of these impacts would benefit from improved understanding of forest and cloud interaction which could be facilitated by the cooperation of remote sensing of high spatial-temporal resolutions and climate models that can better characterize mesoscale cloud processes.

Data and Methods

Cloud cover and environmental datasets

The monthly mean MODIS cloud fraction at 0.05° used in this study was computed from the daily cloud mask data (“cloudy” label for the bits 0-1 of 'state_1km' band) included in the MODIS Surface Reflectance product (MYD09GA.006, overpass at local time of 13:30) of Aqua from 2002 to 2018, using reduceResolution function with “mean” aggregation method on Google Earth Engine (https://earthengine.google.com/). The 1km cloud mask was produced based on the MOD35_L2 cloud mask product which had been extensively validated[56,57]. Before computing cloud fractions, a snow/ice flag

(the bit 12 of 'state_1km' band) was used to remove snow or ice pixels in the cloud record because the high reflectivity of snow/ice degrades the accuracy of cloud detection, especially druing winter in the northern hemisphere. Therefore, the estimated cloud effect would have larger uncertainty in boreal winter than in summer.

To complement MODIS-based cloud analyses, we used the Meteosat Second Generation (MSG) hourly cloud fraction data from June, July and August (JJA) of 2004-2013 at a spatial resolution of 0.05°. The resulting cloud effects and timing statistics were converted to local time.

The cloud fraction from Sentinel-5P Near Real-Time (NRTI) data product was used in this analysis. This dataset is available from 2018-07-05 at a spatial resolution of 0.01° and it has an overpass time of 13:30 similar to MODIS. The Sentinel-5P cloud data, although having a short time span of two years, were useful to separate cloud effects of forest into different cloud types, with the help of a cloud classification scheme based on cloud top pressure and cloud optical depth information[26].

Environmental variables include evapotranspiration (ET, MOD16A2 V6), land surface temperature (LST, MYD11A1 V6) from MODIS, and soil moisture (SM) from the TerraClimate dataset. All these environmental variables were averaged into monthly means at 0.05° resolution.

Elevation data are from SRTM Digital Elevation Data at 0.05° resolution. Land cover data include MODIS (MOD12C1) and European Space Agency (ESA) global land cover products which were aggregated to 0.05°.

Defining forest cover change

To define forest/nonforest and forest cover change, we used the Global forest cover (GFC) product which provides global tree cover for the year 2000 (baseline), yearly forest loss from 2001 to 2018, and forest gain from 2000–2012 at 30m resolution[44]. The GFC data were aggregated to fractions at 0.05°. Net forest cover change was calculated as the sum of the loss and gain accumulated throughout the study period. Pixels with net forest cover change fraction smaller than 0.05 are considered to be "unchanged" and greater than 0.05 are considered to be "changed". Unchanged forest and unchanged nonforest were defined as pixels with baseline tree cover fraction greater or less than 0.5 and with net forest change <

0.05. For unchanged nonforests, pixels classified as water, snow/ice, and wetland were excluded using the major composite of MODIS land cover from 2002 to 2005 with IGBP classification scheme. For "changed" forest pixels, forest loss was identified as those with a net forest loss > 0.15. Forest loss defined this way is expected to pose a stronger signal on clouds than that with a lower threshold, and thus improves the detectability of cloud impact against natural variability of cloud cover.

Estimating potential and actual impacts of forest loss on cloud cover

The potential effect of forest on cloud (ΔCloud) was quantified as the mean cloud difference between unchanged forest and nearby nonforest as:

$$\Delta Cloud = Cloud_{forest} - Cloud_{nonforest} \quad (1)$$

where $Cloud_{forest}$ and $Cloud_{nonforest}$ are multi-year or yearly mean cloud fractions averaged over unchanged forest and unchanged nonforest pixels, respectively. ΔCloud defined this way, with the reversed sign, represents the potential impact of forest loss on cloud cover at a given location. The methodology is designed to isolate the cloud effects of land surface conditions from those caused by meteorological conditions. It refers to local cloud impact (caused by land surface conditions) because effects from synoptic conditions and large-scale circulation changes/climate changes (meteorological conditions), which are shared by both forest and nonforest, are minimized through subtraction. If there is no effect of forest on cloud cover, the resulting ΔCloud would show random patterns with mixed positive and negative values, instead of any systematic patterns which indicate a cloud preference over forest or nonforest.

To implement Eq. 1, we used a moving window approach to search for comparison samples between forest and nearby nonforest pixels at locations underwent "forest change" (i.e., net forest change > 0.05) across the globe[58]. Each moving window was sized at 9 × 9 pixels (0.45° × 0.45°) and two adjacent windows were half-overlapped with a distance of 5 pixels (i.e., the center of two windows was 5-pixels apart along latitudinal and longitudinal direction). To avoid cloud inhibition effects from water bodies such as river/lake[59], water pixels and their one-pixel buffer zone were masked out in the window searching strategy for ΔCloud. Therefore, ΔCloud can be calculated using unchanged forest and nonforest

pixels within each moving window. This window searching strategy ensures the proximity of forest and nonforest pixels to pixels underwent forest change, making the estimated potential effect to be more representative of the actual forest change impact. To test the sensitivity of ΔCloud to window size and time period, ΔCloud was also estimated using alternative window sizes: 11 × 11 (0.55° × 0.55°), 21 × 21 (1.05° × 1.05°), 51 × 51 (2.55° × 2.55°) pixels and different time periods (2002-2007, 2008-2013, 2014-2018). The resulting ΔCloud was similar to results with window size of 9 × 9 (0.45° × 0.45°) and among splitted time periods (Figs. S1 and S2).

A similar window searching strategy was applied to estimate the differences between forest and nonforest in LST (ΔLST), ET (ΔET), and soil moisture (ΔSM) (Fig. S9).

The cloud impact estimated as the cloud differences between forest and nonforest could be confounded by their differences in topography, since topography is known to be an important factor for cloud formation. For example, forests tend to be located in areas with higher elevation and more complex terrain than nonforest. To minimize the topographic influence, we calculated standard deviation (s.d.) of elevation within each moving window and removed samples with s.d. > 100m from the analysis. This filtering effectively excluded comparison samples from complex terrain such as mountainous regions so that the retained samples come from relatively flat areas.

The actual effect of forest loss on cloud ($\Delta Cloud_{loss}$) was quantified as cloud difference between forest loss ($Cloud_{loss}$) and nearby unchanged forest pixels ($Cloud_{forest}$) using the same window searching strategy as the potential effect (Eq.2).

$$\Delta Cloud_{loss} = Cloud_{loss} - Cloud_{forest} \qquad (2)$$

where $\Delta Cloud_{loss}$ is the actual impact of forest loss on cloud, $Cloud_{loss}$ and $Cloud_{forest}$ are the multiyear or yearly mean cloud cover averaged over forest loss and unchanged forest pixels, respectively. The actual impact (deforested vs. forest) shows good spatial resemblance to the potential effect (nonforest vs. forest, ΔCloud with the reversed sign), suggesting that potential effect is able to provide *a priori* prediction of possible cloud change induced by forest loss (R=0.44).

To quantify the progressive tree cover changes caused by forest loss, we calculated tree cover

differences between forest loss and unchanged forest pixels following Eq. 3,

$$\Delta Tree_{year} = (Tree2000_{loss} - Tree2000_{forest}) + \sum_{2001}^{year} (Treeloss_{loss} - Treeloss_{forest}) \quad (3)$$

where $\Delta Tree_{year}$ is the tree cover difference between forest loss and unchanged forest pixels at a given year. It is the sum of the tree cover difference in the baseline year 2000 ($Tree2000_{loss}$ - $Tree2000_{forest}$) and the accumulated yearly forest loss differences from 2001 until a given year (the sigma term of Eq. 3).

The comparison samples obtained from window searching strategy for potential and actual impacts were aggregated to 0.5° for display and further analysis.

Cloud effects of forest separated into different cloud types

By using cloud top pressure and cloud optical depth from the daily Sentinel-5P NRTI data, nine cloud types were classified according to the ISCCP (International Satellite Cloud Climatology Project) cloud classification scheme[26]. The classified cloud types were 1-cirrus, 2-cirrostratus, 3-deep convection, 4-altocumulus, 5-altostratus, 6-nimbostratus, 7-cumulus, 8-stratocumulus, and 9-stratus. Cloud types 1~3, 4~6, and 7~9 corresponded to low, mid- and high-clouds, respectively. Cloud types 3, 7, and 8 were convective clouds and the latter two were shallow convective clouds. The multiyear mean JJA total cloud fraction and fraction of each cloud type were calculated during the available time period and were aggregated to 0.05° from the original 0.01° resolution. We then applied the same moving window method to estimate the cloud effects of forest for total clouds and for different cloud types, respectively. The sumed cloud effects of each cloud type equals the total cloud cover effects. We expected convective cloud types (types 3, 7, and 8) to be influenced by forests, while other non-convective cloud types were not, so that their ΔCloud would show a more random pattern. The dominant cloud type for cloud effects of forest was determined by the cloud type whose ΔCloud had the same sign with the total cloud effects and had the largest magnitude (Fig. S4).

We noted that there were regional differences in the cloud effects estimated from Sentinel-5P and the magnitude of effect was also smaller compared to the other two datasets. For example, the southeast US in MODIS was dominated by negative ΔCloud (64.67%) whereas in Sentinel-5P it showed more

positive ΔCloud (57.09%) (Fig. S12). The large spatial coverage of positive ΔCloud in Europe in MODIS and MSG was slightly reduced with Sentinel-5P. These regional differences might be linked to potential bias in cloud fractions of Sentinel-5P, because we found that cloud fractions of Sentinel-5P were systematically lower than that of both MODIS and MSG (figure not shown). However, the cloud effects of Sentinel-5P in Amazon were consistent with MODIS (72.01%) in terms of coverage, showing a prevailing cloud inhibition (72.68%) (Fig. S12). Cloud inhibition in central Africa (54.63%) was more in line with the widespread negative ΔCloud in MSG (66.43%) than in MODIS (44.02%).

Given these differences in the cloud effects among datasets, the results from Sentinel-5P still provided strong support that convective clouds dominated the cloud effects of forests at both global and regional scales (Fig. S4).

Attribution of cloud effect of forest

Since cloud effects of forest may result from contributions of both vegetation properties and orography, we used tree cover and elevation as indicators to represent each of their effects. Elevation was selected as an indicator of orographic lifting mechanism. We acknowledged that the reality is much more complicated than this highly simplified representation of orographic cloud effect, but for a global scale analysis, elevation could still provide a first-order approximation of orographic effect.

To isolate potential cloud effect of forest into contributions of tree cover and elevation, we first estimated sensitivities of cloud cover to tree cover and elevation, respectively, following a linear regression model defined in Eq. 4.

$$\text{Cloud} = S_{tree} \times \text{tree} + S_{ele} \times \text{elevation} + c \quad (4)$$

where S_{tree} and S_{ele} were the sensitivities of cloud cover to tree cover and elevation, respectively, and the intercept c was unused in this study. The sensitivity parameters were estimated for each moving window separately if it had nonzero tree cover. The estimated slope of cloud cover to elevation (S_{ele}) was positive in the majority of the world (Fig. S8d), suggesting that a higher elevation indeed promotes cloud formation. Next, we calculated tree cover differences (Δtree) and elevation differences (Δele) between unchanged forest and nonforest pixels similarly as the potential effect. Then the cloud differences induced

by tree cover ($\Delta Cloud_{tree}$) and by elevation ($\Delta Cloud_{ele}$) can be obtained by multiplying their sensitivities by the corresponding differences as Eqs 5 and 6. The sensitivity and differences parameters were averaged to 0.5° resolution before used in Eqs. 5 and 6 (Fig. S8).

$$\Delta Cloud_{tree} = S_{tree} \times \Delta tree \quad (5)$$

$$\Delta Cloud_{ele} = S_{ele} \times \Delta ele \quad (6)$$

The reconstructed ΔCloud given by the sum of $\Delta Cloud_{tree}$ and $\Delta Cloud_{ele}$ explained about 70% of the original ΔCloud.

To attribute ΔCloud into tree cover and elevation-induced cloud changes, we compared the sign and magnitude of original ΔCloud, $\Delta Cloud_{tree}$, and $\Delta Cloud_{ele}$. If $\Delta Cloud_{tree}$ and $\Delta Cloud_{ele}$ both have the same sign as ΔCloud, the one with greater magnitude is classified as the dominant factor. If only one of $\Delta Cloud_{tree}$ and $\Delta Cloud_{ele}$ has the same sign as ΔCloud, the factor with the same sign is classified as the dominant factor. If none of $\Delta Cloud_{tree}$ and $\Delta Cloud_{ele}$ have the same sign as ΔCloud, the dominant factor is classified as other. As a result, potential cloud effect can be attributed to five classes: tree cover induced cloud increase (Tree+) and decrease (Tree-), orography induced cloud increase (Orography+) and decrease (Orography-), and other.

Linking cloud effect with sensible heat flux

Sensible heat data were from three independent sources: satellite estimate[4], Community Land Model version 5 simulation[31], and 30 paired forest and nonforest flux sites[32].

Satellite estimates provide changes in the combined sensible heat and ground heat fluxes (H+G) under different land cover conversions at 1° spatial resolution (a total of 45 pairs conversions for "HG_IGBPdet"). The combined fluxes of H+G were estimated as the residual of surface energy components as described in Ref[4]. Due to the small contribution of G to H+G, we referred "H+G" to "H" for simplicity in the following text and the main text. To obtain sensible heat differences between forest and nonforest (ΔH) that are compatible with ΔCloud, we extracted the dominant land cover type for unchanged forest (e.g., evergreen broadleaf) and nonforest pixels (e.g., crop) within each moving window from the ESA land cover product. The dominant land cover types for forest and nonforest were upscaled

to 1° resolution with the "major" method (figure not shown for 1°, but a similar one for 0.5° is shown in Fig. S9). For each one-degree grid box with a dominant forest type (e.g., crop) and nonforest type (e.g., evergreen broadleaf), ΔH can be extracted from the corresponding sensible heat change value that matches the specific land conversion of that grid box (e.g., evergreen broadleaf to crop).

CLM5 is the land component of the state of the art earth system model Community Earth System Model 2 [60]. The CLM5 simulation was conducted at the spatial resolution of 0.5° from 1997 to 2010, driven by a revised climatology GSWP3 as the atmospheric forcing (http://hydro.iis.utokyo.ac.jp/GSWP3/), with a satellite phenology, the land cover of 2000, and the separated soil columns configuration enabled[61,62]. The years 1997 to 2001 were spinup period and excluded from the analysis. We used the subgrid PFT-level (plant functional type) model outputs to calculate sensible heat differences between different land cover types within the same model grid. To match CLM5 model resolution, the dominant land cover types for forest and nonforest of each moving window were upscaled to 0.5° using the ESA land cover data (Fig. S9). Because CLM adopted a different land classification scheme, we created a look-up table to convert CLM land cover to IGBP classification scheme (Table S1). The differences in sensible heat change (ΔH) between specific forest and nonforest types can be extracted from the corresponding sensible heat values of different land cover types in the model grid.

A total of 30 paired flux sites were used in this study to calculate sensible heat differences between nonforest and forest (ΔH). Twenty eight site pairs were processed by Ref[32] using FLUXNET data and two additional Amazon site pairs were from the ORNL archive[63] (Table S2). ΔH was calculated using the mean sensible heat flux during the daytime (8:00 to 16:00). ΔCloud for each site pair was extracted from the centered location of the line linking two sites. Unlike ΔCloud used in the main analysis which was aggregated to 0.5°, we here used ΔCloud aggregated to 1° without the elevation s.d. criteria and one-pixel water buffer removal to increase available ΔCloud value for each site pair. When analyzing the relationship between ΔH and ΔCloud, two flux pairs were excluded because of the missing of matched ΔCloud (pair 29) and an outlier in ΔH (pair 22 with ΔH >200W/m^2).

Scale-dependency of potential cloud effect of forest

To investigate how the potential cloud effect varies with spatial scale, we reprocessed the MODIS cloud cover and GFC data into different spatial resolutions to emulate the scale change (using "mean" for cloud cover and "major" method for forest cover). Specifically, the 0.05° cloud and GFC data used in the main analysis were aggregated to coarser resolutions (0.1°, 0.25°, 0.5° and 1°) and ΔCloud was re-estimated with window searching strategy of slightly different configurations to accommodate the resolution change (Fig. S11). The specific parameters of window searching strategy under different resolutions are provided in Table S3, including raw data resolution, window size, window distance, and display resolution. For a given resolution, ΔCloud was estimated with two parameter combinations to ensure the robustness of the results.

Acknowledgements

This study is supported by the National Key Research and Development Program of China (No. 2017YFA0604701) and the Fundamental Research Funds for the Central Universities. We would like to thank the high-performance computing support from the Center for Geodata and Analysis, Faculty of Geographical Science, Beijing Normal University [https://gda.bnu.edu.cn/].

Author contribution

Y.L. conceived and designed the study; R.X. and Y.L. performed the data analysis; Y.L., R.X., A.J.T., and L.Z. analyzed the results, with help from D.V.S, L.G., R.M., L.C., Y.Z. in interpretation of the results; Y.L. and R.X. wrote the manuscript with contributions from all authors. R.M. conducted the CLM5 simulation; L.C. provided the flux tower data.

Competing financial interests

The authors declare no competing financial interests.

Data Availability

Code and data needed to reproduce this study will be available at Figshare.

References

1. Bonan, G. B. Forests and climate change: Forcings, feedbacks, and the climate benefits of forests. *Science (80-.).* **320**, 1444–1449 (2008).
2. Runyan, C., D'Odorico, P. & Lawrence, D. Physical and biological feedbacks of deforestation. *Rev. Geophys.* **50**, 1–32 (2012).
3. Lee, X. *et al.* Observed increase in local cooling effect of deforestation at higher latitudes. *Nature* **479**, 384–387 (2011).
4. Duveiller, G., Hooker, J. & Cescatti, A. The mark of vegetation change on Earth's surface energy balance. *Nat. Commun.* **9**, (2018).
5. Li, Y. *et al.* Local cooling and warming effects of forests based on satellite observations. *Nat. Commun.* **6**, 6603 (2015).
6. Norris, J. R. *et al.* Evidence for climate change in the satellite cloud record. *Nature* **536**, 72–75 (2016).
7. Lucia, P. *et al.* Biophysical effects on temperature and precipitation due to land cover change. *Environ. Res. Lett.* **12**, 53002 (2017).
8. Spracklen, D. V. & Garcia-Carreras, L. The impact of Amazonian deforestation on Amazon basin rainfall. *Geophys. Res. Lett.* **42**, 9546–9552 (2015).
9. Winckler, J., Reick, C. H. & Pongratz, J. Robust identification of local biogeophysical effects of land-cover change in a global climate model. *J. Clim.* **30**, 1159–1176 (2017).
10. Branch, O. & Wulfmeyer, V. Deliberate enhancement of rainfall using desert plantations. *Proc. Natl. Acad. Sci.* **116**, 18841–18847 (2019).
11. Chen, L. & Dirmeyer, P. A. Reconciling the disagreement between observed and simulated temperature responses to deforestation. *Nat. Commun.* **11**, 202 (2020).
12. Winckler, J., Lejeune, Q., Reick, C. H. & Pongratz, J. Nonlocal Effects Dominate the Global Mean Surface Temperature Response to the Biogeophysical Effects of Deforestation. *Geophys. Res. Lett.* **46**, 745–755 (2019).
13. Lawrence, D. & Vandecar, K. Effects of tropical deforestation on climate and agriculture. *Nat. Clim. Chang.* **5**, 27–36 (2014).
14. Baidya Roy, S. & Avissar, R. Impact of land use/land cover change on regional hydrometeorology in Amazonia. *J. Geophys. Res.* **107**, (2002).

15. Wang, J., Bras, R. L. & Eltahir, E. A. B. The Impact of Observed Deforestation on the Mesoscale Distribution of Rainfall and Clouds in Amazonia. *J. Hydrometeorol.* **1**, 267–286 (2000).

16. Negri, A., Adler, R., Xu, L. & Surratt, J. The impact of Amazonian deforestation on dry season rainfall. *J. Clim.* **17**, 1306–1319 (2004).

17. Wang, J. *et al.* Impact of deforestation in the Amazon basin on cloud climatology. *Proc. Natl. Acad. Sci.* **106**, 3670–3674 (2009).

18. Souza, E. P., Renno, N. O. & Dias, M. A. F. S. Convective circulations induced by surface heterogeneities. *J. Atmos. Sci.* **57**, 2915–2922 (2000).

19. Garcia-Carreras, L., Parker, D. J., Taylor, C. M., Reeves, C. E. & Murphy, J. G. Impact of mesoscale vegetation heterogeneities on the dynamical and thermodynamic properties of the planetary boundary layer. *J. Geophys. Res. Atmos.* **115**, 1–12 (2010).

20. Snyder, P. K., Delire, C. & Foley, J. A. Evaluating the influence of different vegetation biomes on the global climate. *Clim. Dyn.* **23**, 279–302 (2004).

21. Teuling, A. J. *et al.* Observational evidence for cloud cover enhancement over western European forests. *Nat. Commun.* **8**, 14065 (2017).

22. Nair, U. S. Impact of land use on Costa Rican tropical montane cloud forests: Sensitivity of cumulus cloud field characteristics to lowland deforestation. *J. Geophys. Res.* **108**, 4206 (2003).

23. Hohenegger, C. & Stevens, B. The role of the permanent wilting point in controlling the spatial distribution of precipitation. *Proc. Natl. Acad. Sci.* **115**, 5692–5697 (2018).

24. Taylor, C. M., De Jeu, R. A. M., Guichard, F., Harris, P. P. & Dorigo, W. A. Afternoon rain more likely over drier soils. *Nature* **489**, 423–426 (2012).

25. D'Almeida, C. & Vörösmarty, C. The effects of deforestation on the hydrological cycle in Amazonia: a review on scale and resolution. *Int. J. Climatol.* **27**, 633–647 (2007).

26. Rossow, W. B. *Climate Data Record (CDR) Program: Climate Algorithm Theoretical Basis Document (C-ATBD) International Satellite Cloud Climatology Project (ISCCP) Cloud Properties - ISCCP (H-Series Product)*. (2017).

27. Sandel, B. & Svenning, J.-C. Human impacts drive a global topographic signature in tree cover. *Nat. Commun.* **4**, 2474 (2013).

28. Houze, R. A. Orographic effects on precipitating clouds. *Rev. Geophys.* **50**, RG1001 (2012).

29. Angleton, G. M. & Bonham, C. D. Least squares regression vs. geometric mean regression for ecotoxicology studies. *Appl. Math. Comput.* **72**, 21–32 (1995).

30. Bosman, P. J. M., van Heerwaarden, C. C. & Teuling, A. J. Sensible heating as a potential mechanism for enhanced cloud formation over temperate forest. *Q. J. R. Meteorol. Soc.* 450–468 (2018). doi:10.1002/qj.3441

31. Meier, R., Davin, E. L., Swenson, S. C., Lawrence, D. M. & Schwaab, J. Biomass heat storage

dampens diurnal temperature variations in forests. *Environ. Res. Lett.* **14**, 084026 (2019).

32. Chen, L., Dirmeyer, P. A., Guo, Z. & Schultz, N. M. Pairing FLUXNET sites to validate model representations of land-use/land-cover change. *Hydrol. Earth Syst. Sci.* **22**, 111–125 (2018).

33. von Randow, C. *et al.* Comparative measurements and seasonal variations in energy and carbon exchange over forest and pasture in South West Amazonia. *Theor. Appl. Climatol.* **78**, 5–26 (2004).

34. Li, Y. *et al.* The role of spatial scale and background climate in the latitudinal temperature response to deforestation. *Earth Syst. Dyn.* **7**, 167–181 (2016).

35. Bright, R. M. *et al.* Local temperature response to land cover and management change driven by non-radiative processes. *Nat. Clim. Chang.* **7**, 296–302 (2017).

36. Spracklen, D. V., Arnold, S. R. & Taylor, C. M. Observations of increased tropical rainfall preceded by air passage over forests. *Nature* **489**, 282–285 (2012).

37. Heiblum, R. H., Koren, I. & Feingold, G. On the link between Amazonian forest properties and shallow cumulus cloud fields. *Atmos. Chem. Phys.* **14**, 6063–6074 (2014).

38. Fisch, G. *et al.* The convective boundary layer over pasture and forest in Amazonia. *Theor. Appl. Climatol.* **78**, 47–59 (2004).

39. Chen, F. & Avissar, R. Impact of Land-Surface Moisture Variability on Local Shallow Convective Cumulus and Precipitation in Large-Scale Models. *J. Appl. Meteorol.* **33**, 1382–1401 (1994).

40. Gambill, L. D. & Mecikalski, J. R. A Satellite-Based Summer Convective Cloud Frequency Analysis over the Southeastern United States. *J. Appl. Meteorol. Climatol.* **50**, 1756–1769 (2011).

41. Gentine, P., Holtslag, A. A. M., D'Andrea, F. & Ek, M. Surface and Atmospheric Controls on the Onset of Moist Convection over Land. *J. Hydrometeorol.* **14**, 1443–1462 (2013).

42. Khanna, J., Medvigy, D., Fueglistaler, S. & Walko, R. Regional dry-season climate changes due to three decades of Amazonian deforestation. *Nat. Clim. Chang.* **7**, 200–204 (2017).

43. Curtis, P. G., Slay, C. M., Harris, N. L., Tyukavina, A. & Hansen, M. C. Classifying drivers of global forest loss. *Science (80-.).* **361**, 1108–1111 (2018).

44. Hansen, M., Potapov, P. & Moore, R. High-resolution global maps of 21st-century forest cover change. *Science (80-.).* **850**, 850–853 (2013).

45. Taubert, F. *et al.* Global patterns of tropical forest fragmentation. *Nature* **554**, 519–522 (2018).

46. Maeda, E. E. *et al.* Large-scale commodity agriculture exacerbates the climatic impacts of Amazonian deforestation. *Proc. Natl. Acad. Sci.* **118**, e2023787118 (2021).

47. Garcia-Carreras, L. & Parker, D. J. How does local tropical deforestation affect rainfall? *Geophys. Res. Lett.* **38**, 1–6 (2011).

48. Knox, R., Bisht, G., Wang, J. & Bras, R. Precipitation variability over the forest-to-nonforest transition in Southwestern Amazonia. *J. Clim.* **24**, 2368–2377 (2011).

49. Vergopolan, N. & Fisher, J. B. The impact of deforestation on the hydrological cycle in Amazonia as observed from remote sensing. *Int. J. Remote Sens.* **37**, 5412–5430 (2016).

50. Harrop, B. E., Ma, P. L., Rasch, P. J., Neale, R. B. & Hannay, C. The Role of Convective Gustiness in Reducing Seasonal Precipitation Biases in the Tropical West Pacific. *J. Adv. Model. Earth Syst.* (2018). doi:10.1002/2017MS001157

51. Reyer, C. P. O. *et al.* Forest resilience and tipping points at different spatio-temporal scales: approaches and challenges. *J. Ecol.* **103**, 5–15 (2015).

52. Pinto, E., Shin, Y., Cowling, S. A. & Jones, C. D. Past, present and future vegetation-cloud feedbacks in the Amazon Basin. *Clim. Dyn.* **32**, 741–751 (2009).

53. Allen, C. D., Breshears, D. D. & McDowell, N. G. On underestimation of global vulnerability to tree mortality and forest die-off from hotter drought in the Anthropocene. *Ecosphere* **6**, 1–55 (2015).

54. van der Ent, R. J., Savenije, H. H. G., Schaefli, B. & Steele-Dunne, S. C. Origin and fate of atmospheric moisture over continents. *Water Resour. Res.* **46**, 1–12 (2010).

55. Betts, M. G. *et al.* Global forest loss disproportionately erodes biodiversity in intact landscapes. *Nature* (2017). doi:10.1038/nature23285

56. Frey, R. A. *et al.* Cloud Detection with MODIS. Part I: Improvements in the MODIS Cloud Mask for Collection 5. *J. Atmos. Ocean. Technol.* **25**, 1057–1072 (2008).

57. Ackerman, S. A. *et al.* Cloud Detection with MODIS. Part II: Validation. *J. Atmos. Ocean. Technol.* **25**, 1073–1086 (2008).

58. Li, Y. *et al.* Potential and Actual impacts of deforestation and afforestation on land surface temperature. *J. Geophys. Res. Atmos.* **121**, 14372–14386 (2016).

59. Segal, M. *et al.* On the Clearing of Cumulus Clouds Downwind from Lakes. *Mon. Weather Rev.* **125**, 639–646 (1997).

60. Lawrence, D. *et al.* Technical description of version 5.0 of the Community Land Model (CLM). *NCAR/TN-478+STR NCAR Tech. Note* (2018).

61. Meier, R. *et al.* Evaluating and improving the Community Land Model's sensitivity to land cover. *Biogeosciences* **15**, 4731–4757 (2018).

62. Schultz, N. M., Lee, X., Lawrence, P. J., Lawrence, D. M. & Zhao, L. Assessing the use of subgrid land model output to study impacts of land cover change. *J. Geophys. Res. Atmos.* **121**, 6133–6147 (2016).

63. SALESKA, S. R. *et al.* LBA-ECO CD-32 Flux Tower Network Data Compilation, Brazilian Amazon: 1999-2006. (2013). doi:10.3334/ORNLDAAC/1174

Supplmentary information

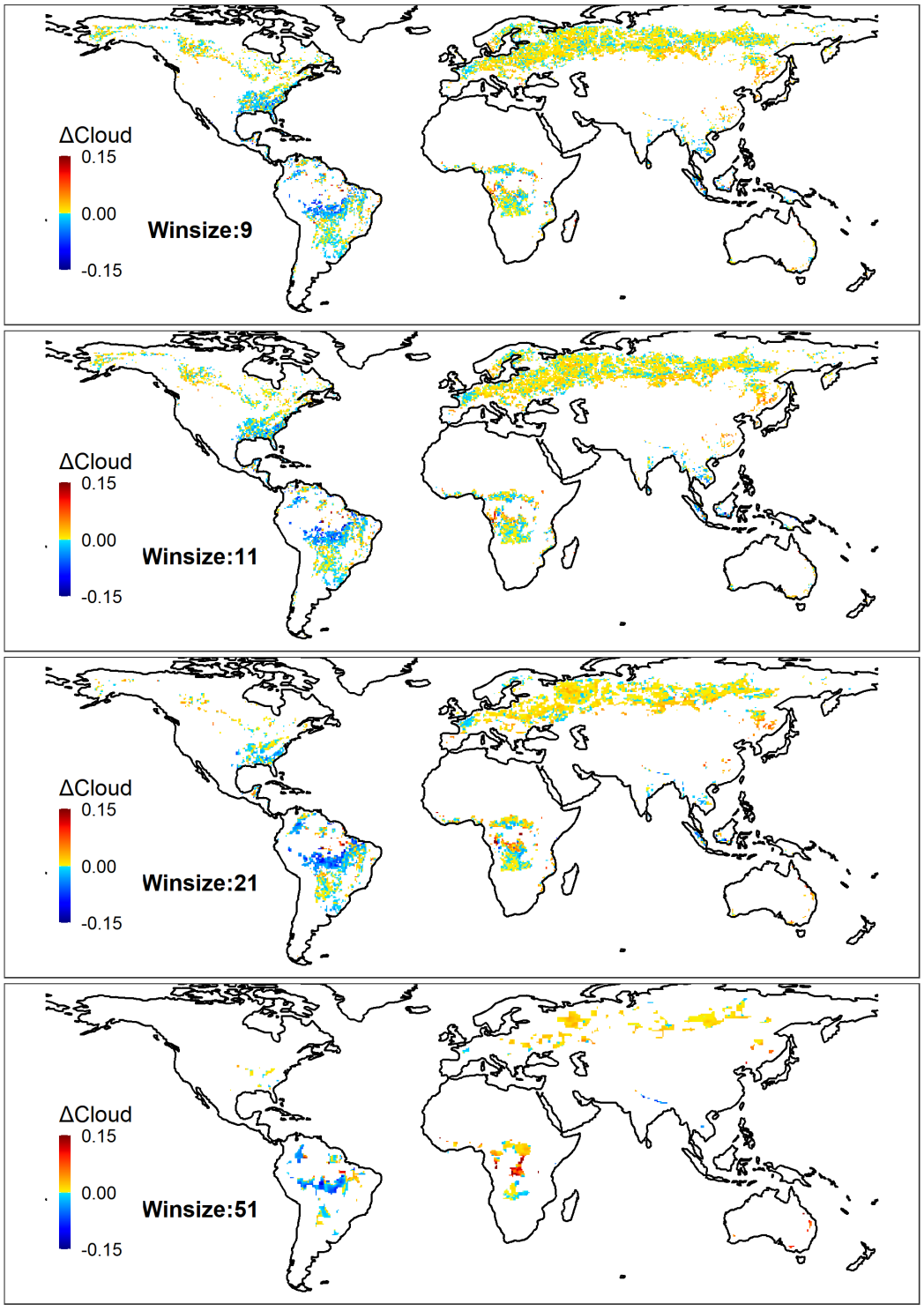

Figure S1. Potential effects of forest on June-August (JJA) cloud cover based on MODIS data at 0.05° resolution estimated using different window sizes: (a) 9×9 (0.45° × 0.45°), (b) 11×11 (0.55° × 0.55°), (c) 21×21 (1.05° × 1.05°), and (d) 51×51 (2.55° × 2.55°).

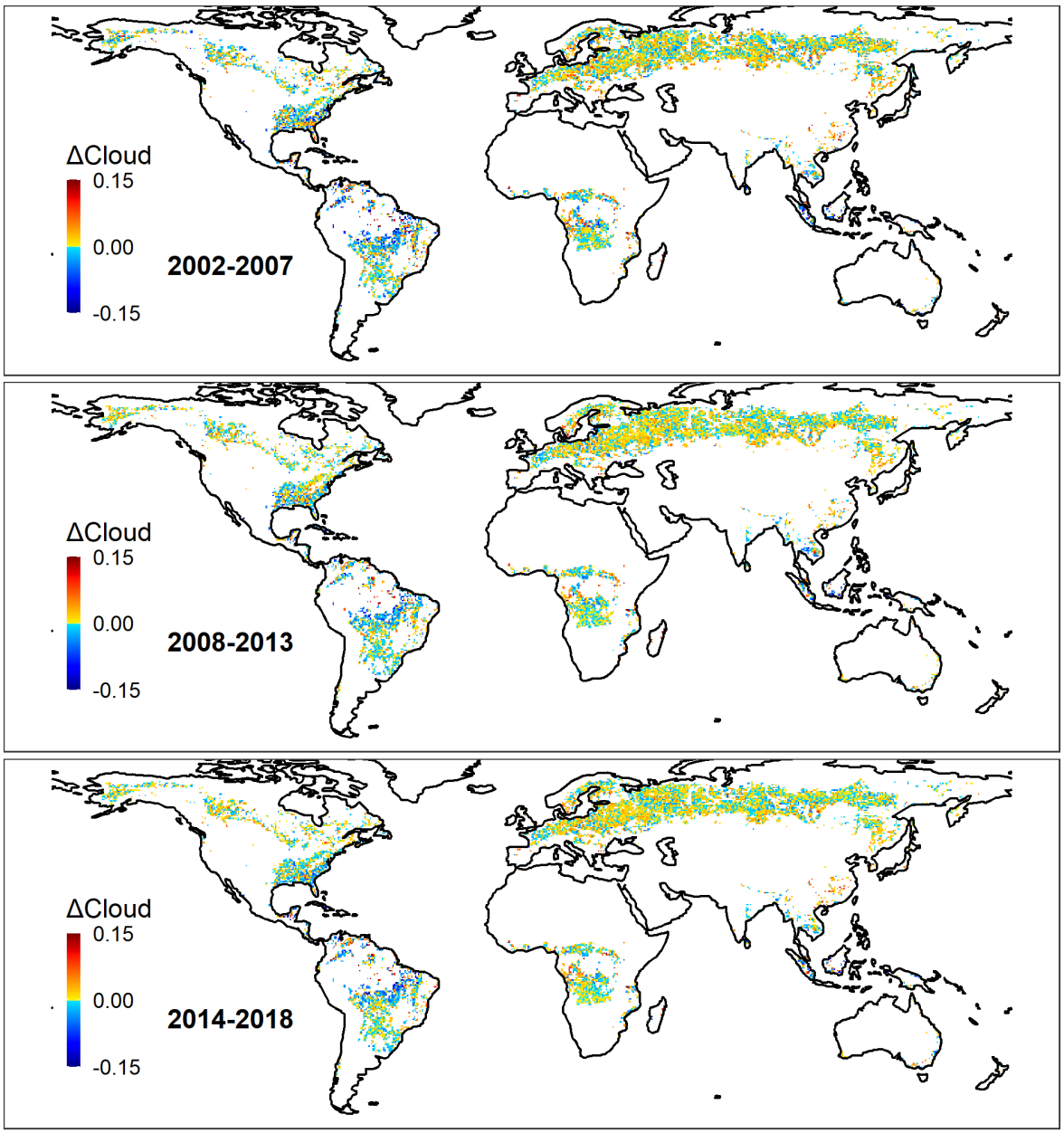

646 Figure S2. Potential effects of forest on June-August (JJA) cloud cover based on MODIS data estimated
647 for different time-periods (a) 2002-2007 (b) 2008-2013 and (c) 2014-2018.

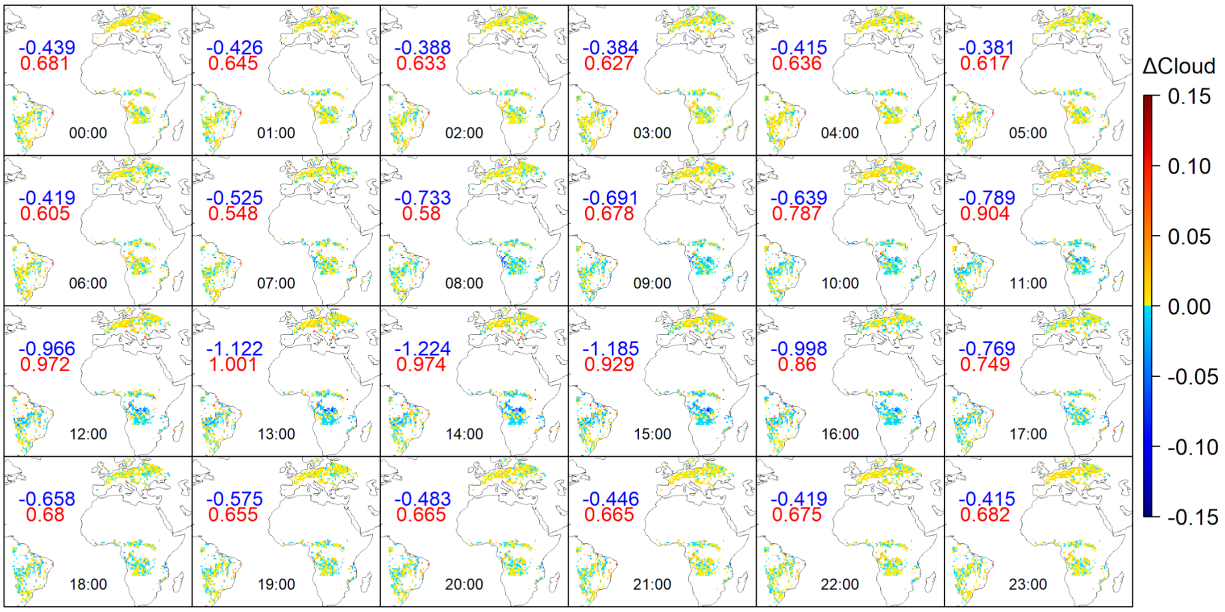

Figure S3. Diurnal variations in the potential effects of forest on JJA cloud cover based on MSG data. The red and blue texts show the averaged positive and negative ΔCloud over the domain, multiplied by 100 for display.

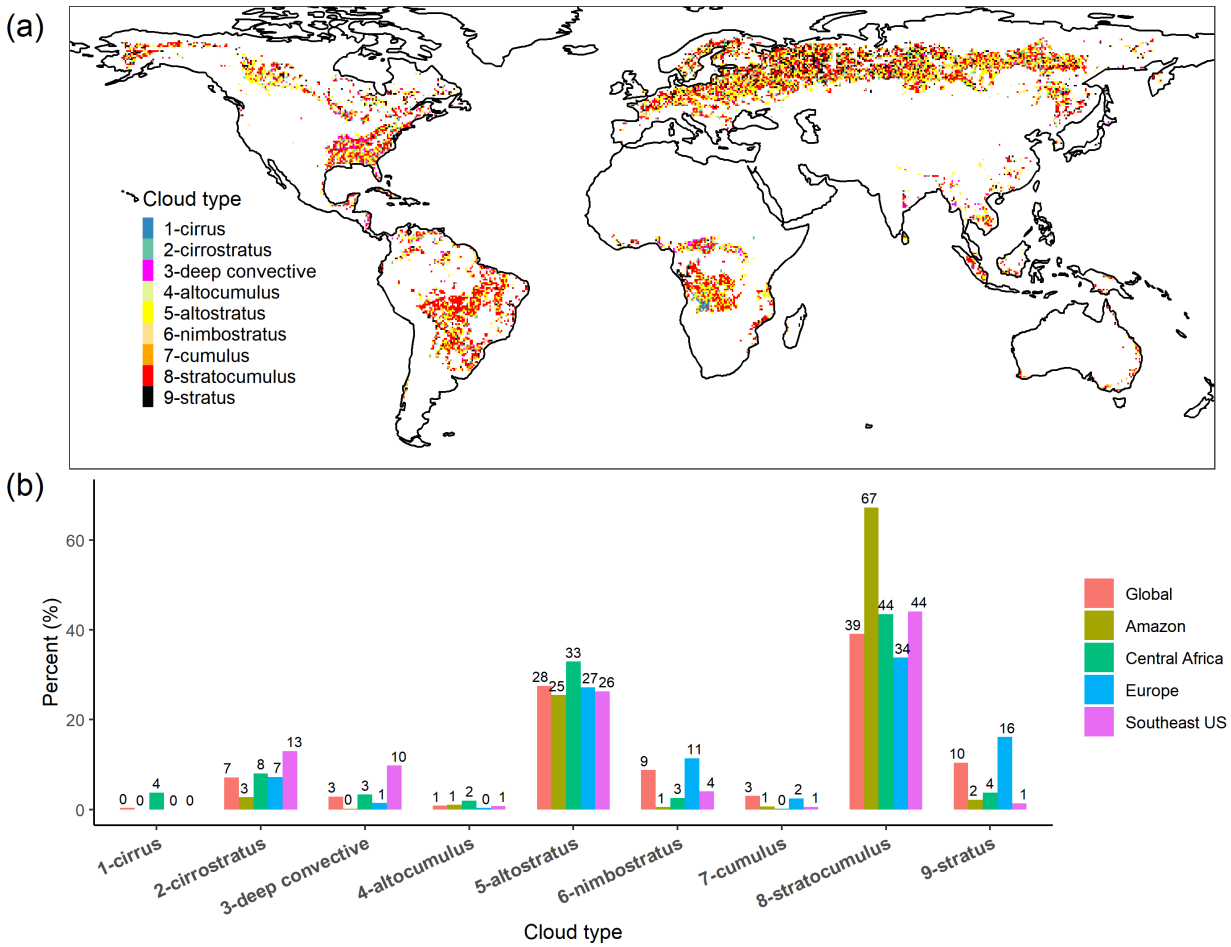

659 Figure S4. (a) The dominant cloud type for the cloud effects of forest in JJA based on Sentinel-5P and (b)
660 the percentage for each dominant type globally and for four selected regions defined in Fig. S12.

661

662

663

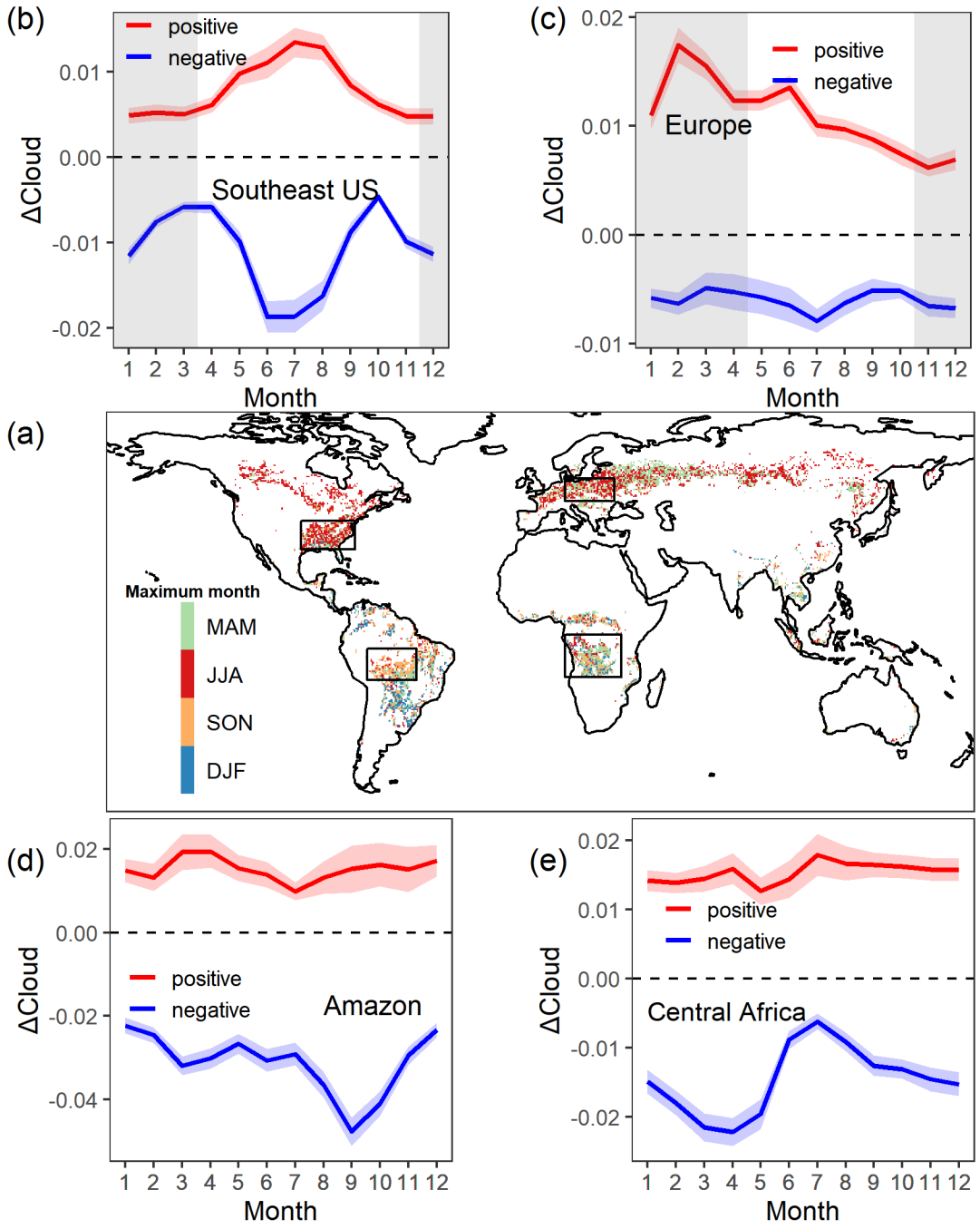

664 Figure S5. (a) Months of the maximum potential cloud effect during snowfree season. Seasonal changes
665 of ΔCloud in (b) Southeast US (lon: -97° to -75°; lat: 30° to 40°), (c) Europe (lon: 10° to 30°; lat: 47° to
666 55°], (d) Amazon (lon: -70° to -50°; lat: -16° to -5°), and (e) Central Africa (lon:10° to 33°; lat: -15° to
667 0°]). Months with snow cover are shown as shaded areas in Panels b-e.

668

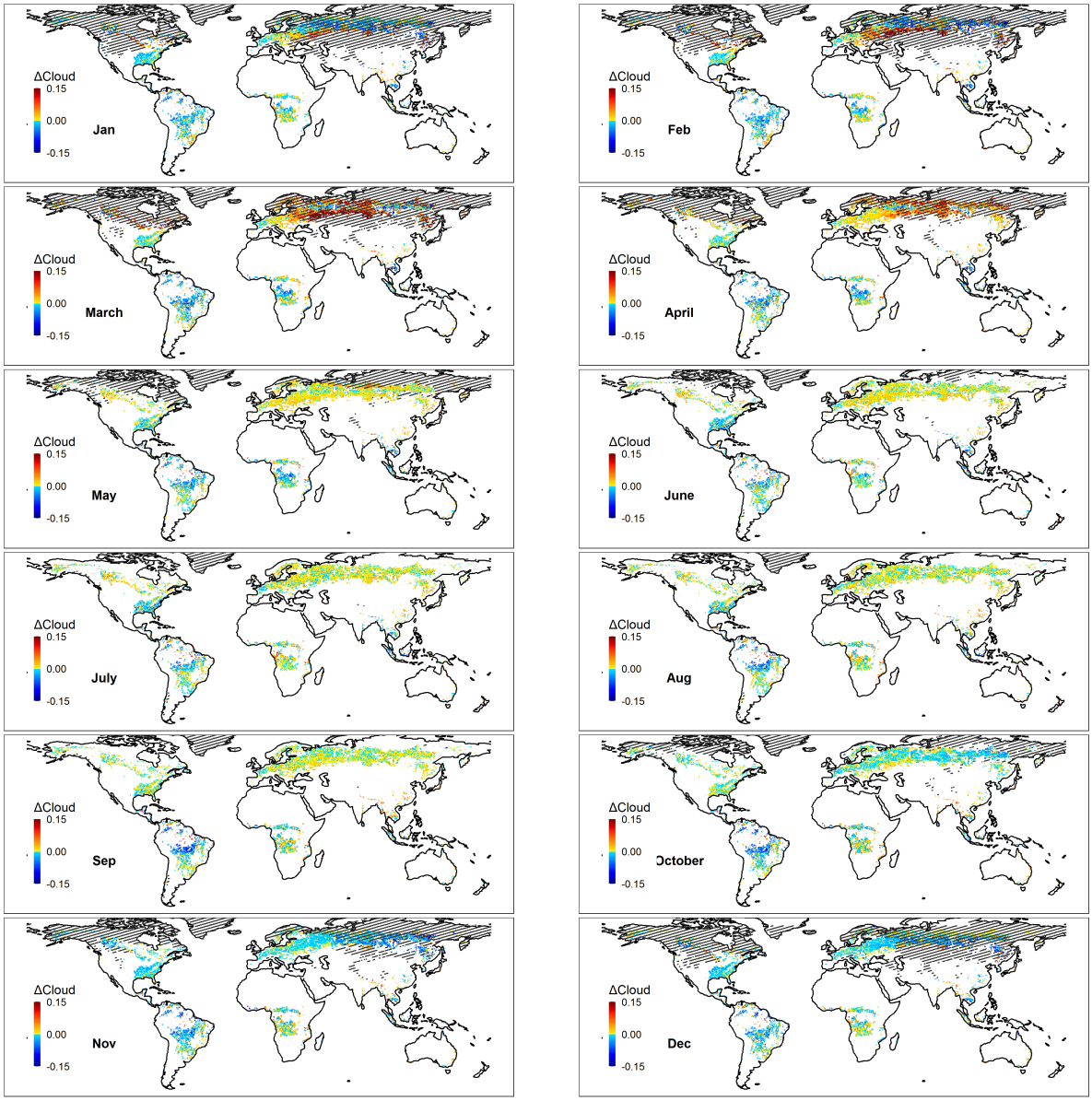

669 Figure S6. Monthly variations in the potential effects of forest on cloud cover based on MODIS data. The
670 presence of snow/ice is denoted as the dashed areas for each month.

671

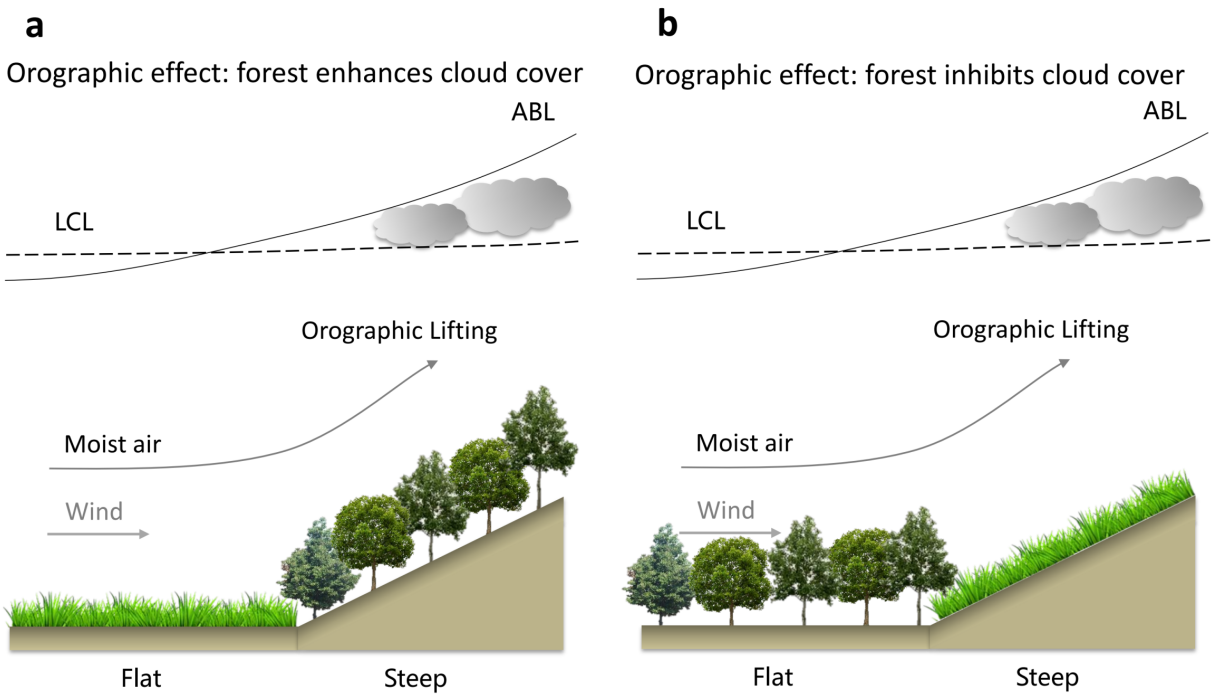

672

673 Figure S7. Schematic of orographic clouds which confound the forest effect on cloud cover. (a)
674 Orographic induced enhanced cloud cover and (b) inhibited cloud cover over forest.

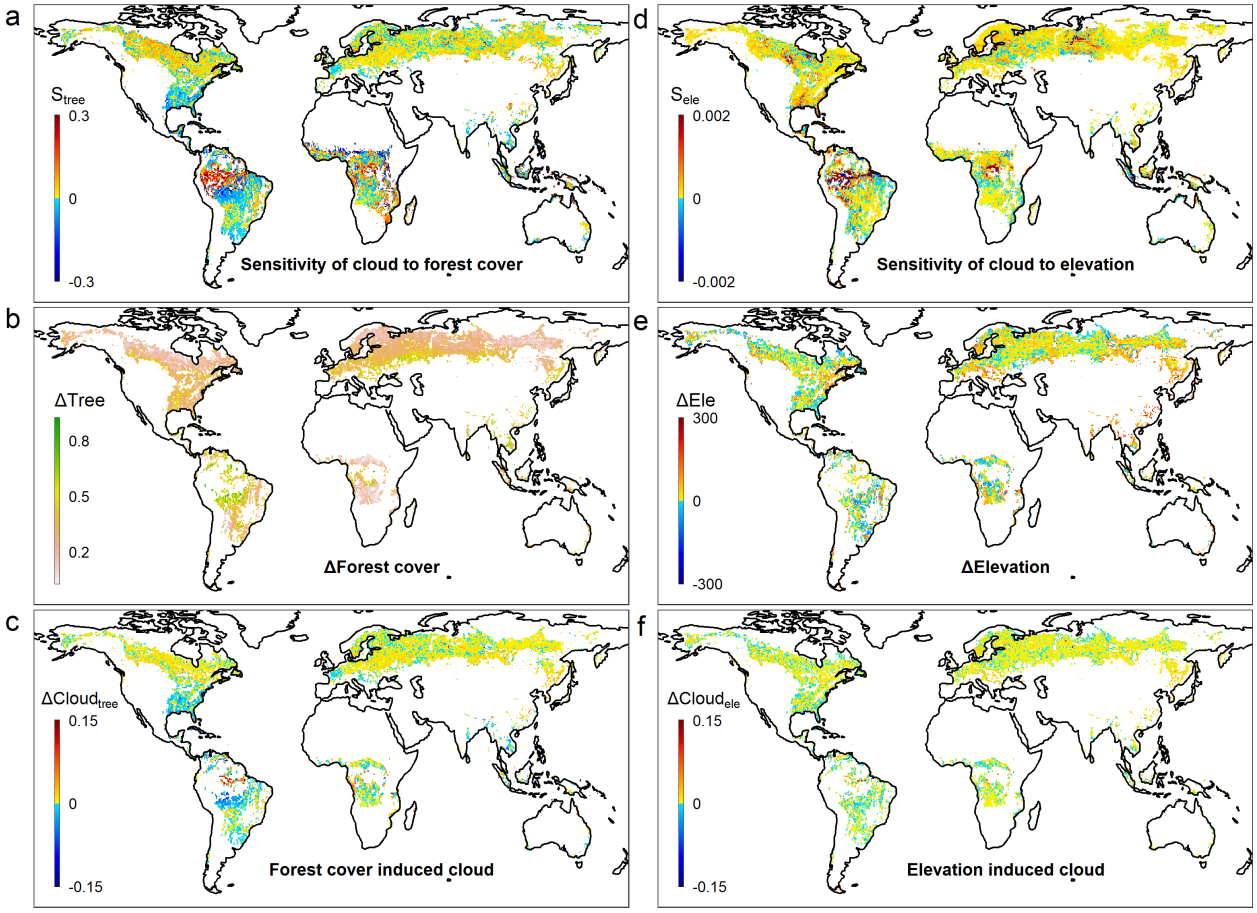

675 Figure S8. Attribution of JJA ΔCloud to tree cover and elevation. (a,d) Sensitivities of cloud cover to tree
676 cover (S_{tree}, unit:fraction/fraction) and elelvation (S_{ele}, unit:fraction/m) estimated using Eq. 4. (b,d)
677 Differences between forest and nonforest in tree cover (ΔTree, unit:fraction) and elevation (Δele, unit:m).
678 (c, f) Tree cover induced cloud differences estimated following Eq. 5 ($\Delta Cloud_{tree}$) and elevation induced
679 cloud differences ($\Delta Cloud_{ele}$) estimated following Eq. 6.

680

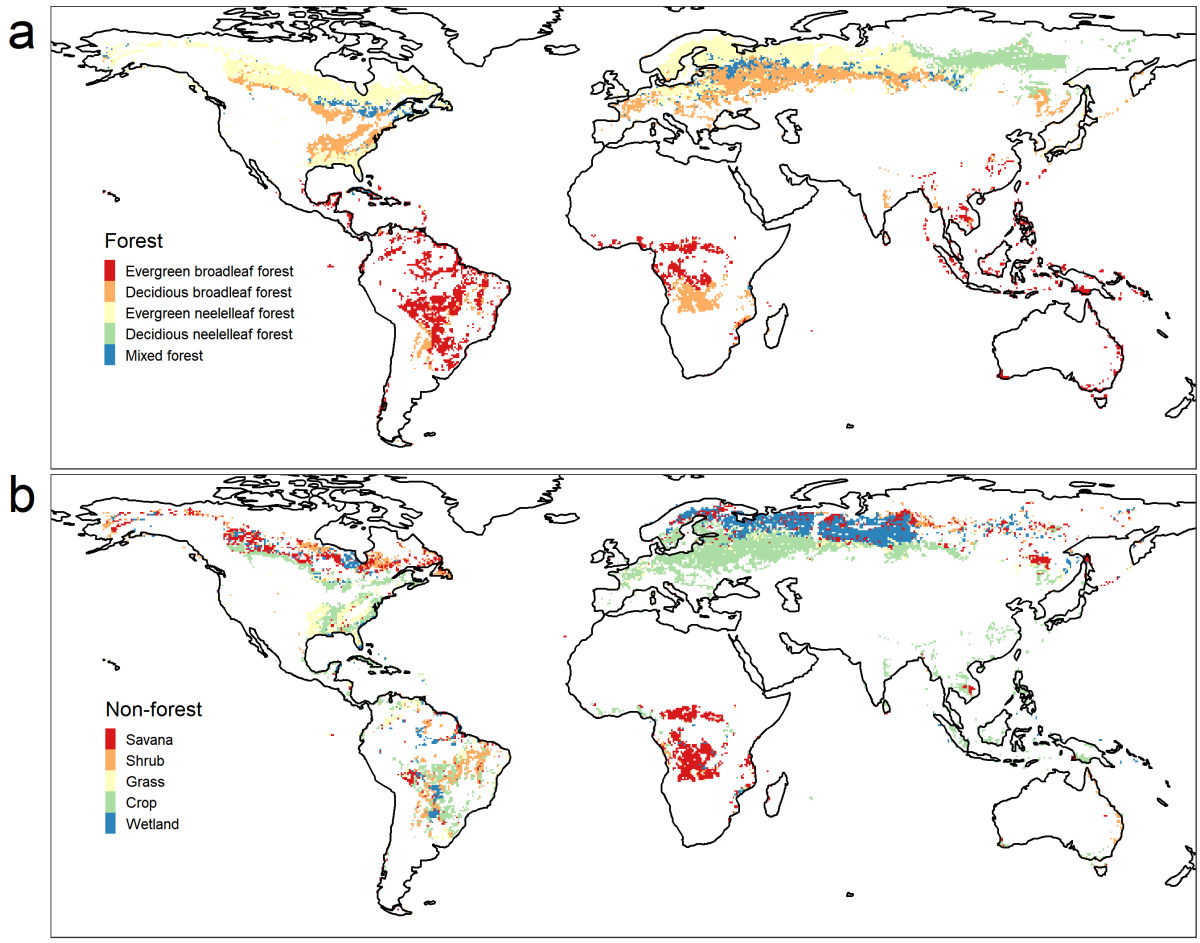

681 Figure S9. Dominant land cover types for (a) forest and (b) nonforest pixels within the 9×9 moving
682 window aggregated to 0.5° resolution. Land cover type information was from the ESA land cover data.

683

684

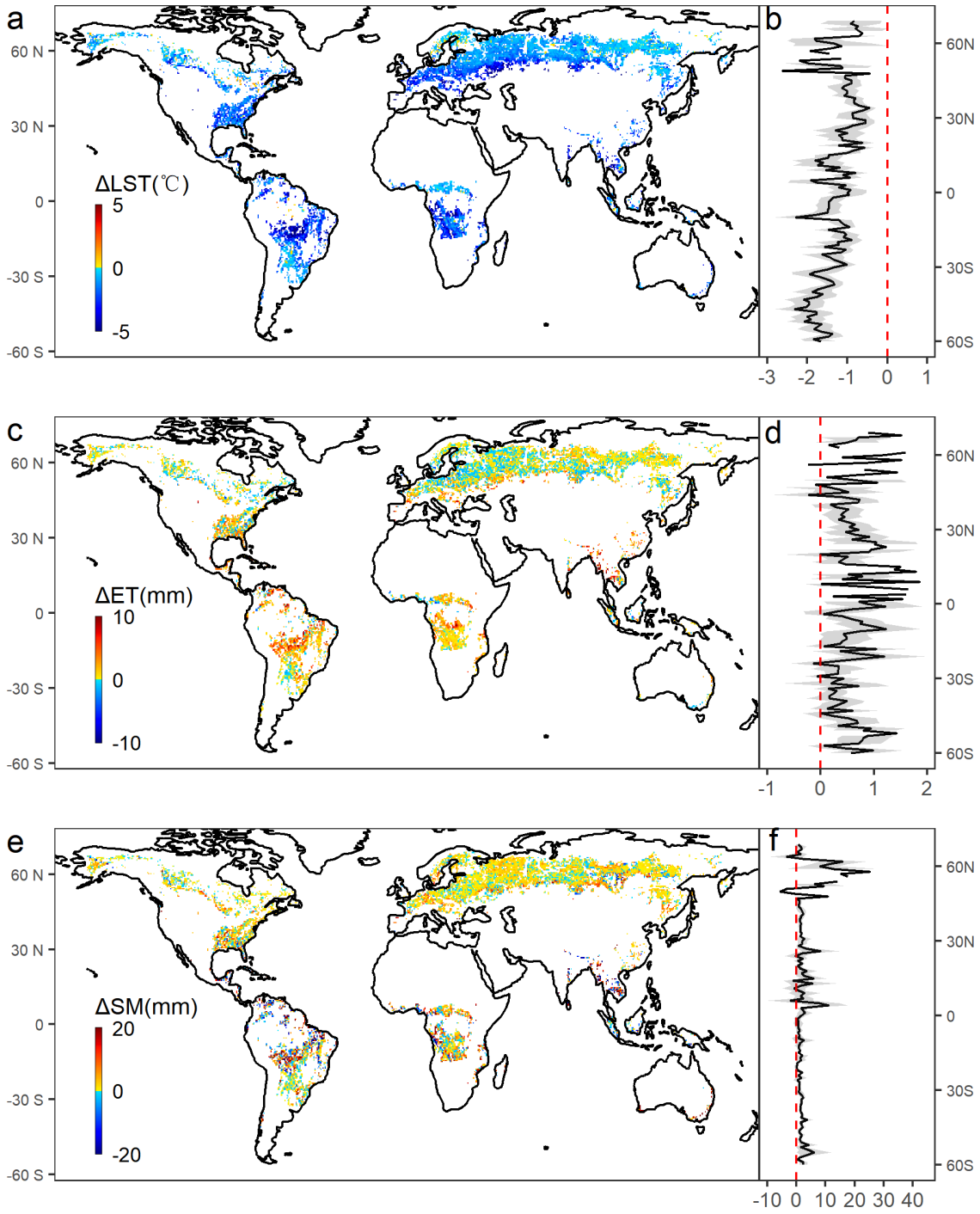

685
686 Figure S10. Mean differences between forest and nonforest in LST (a), ET (c), and soil moisture (e) in
687 JJA from 2002 to 2018 and their latitudinal patterns (b,d,f).

688

689

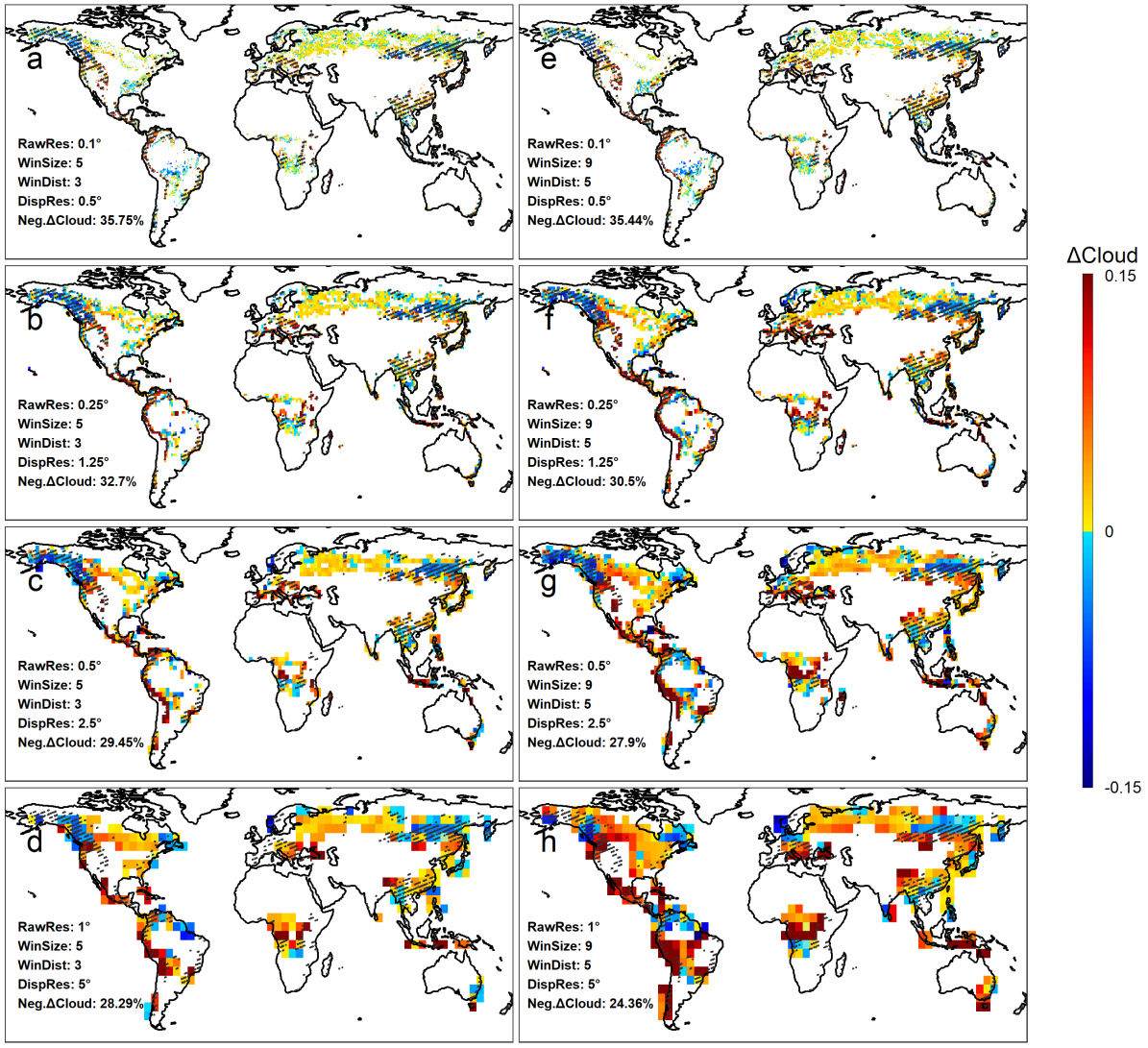

690 Figure S11. Potential cloud effects of forest estimated using MODIS JJA cloud cover data resampled into
691 different spatial resolutions at (a,e) 0.1°, (b,f) 0.25°, (c,g) 0.5°, and (d,h) 1°. Each column shows ΔCloud
692 estimated using different parameter setups for window searching strategy (WinSize and WinDist, see
693 Table S3). Dashed lines on the map show areas with complex topography (elevation sd. >100m) and are
694 excluded in the calculation of percentage of negative ΔCloud (i.e., cloud inhibition). Note that the
695 percentage of negative ΔCloud for different resolutions was calculated without excluding the areas with
696 complex topography.

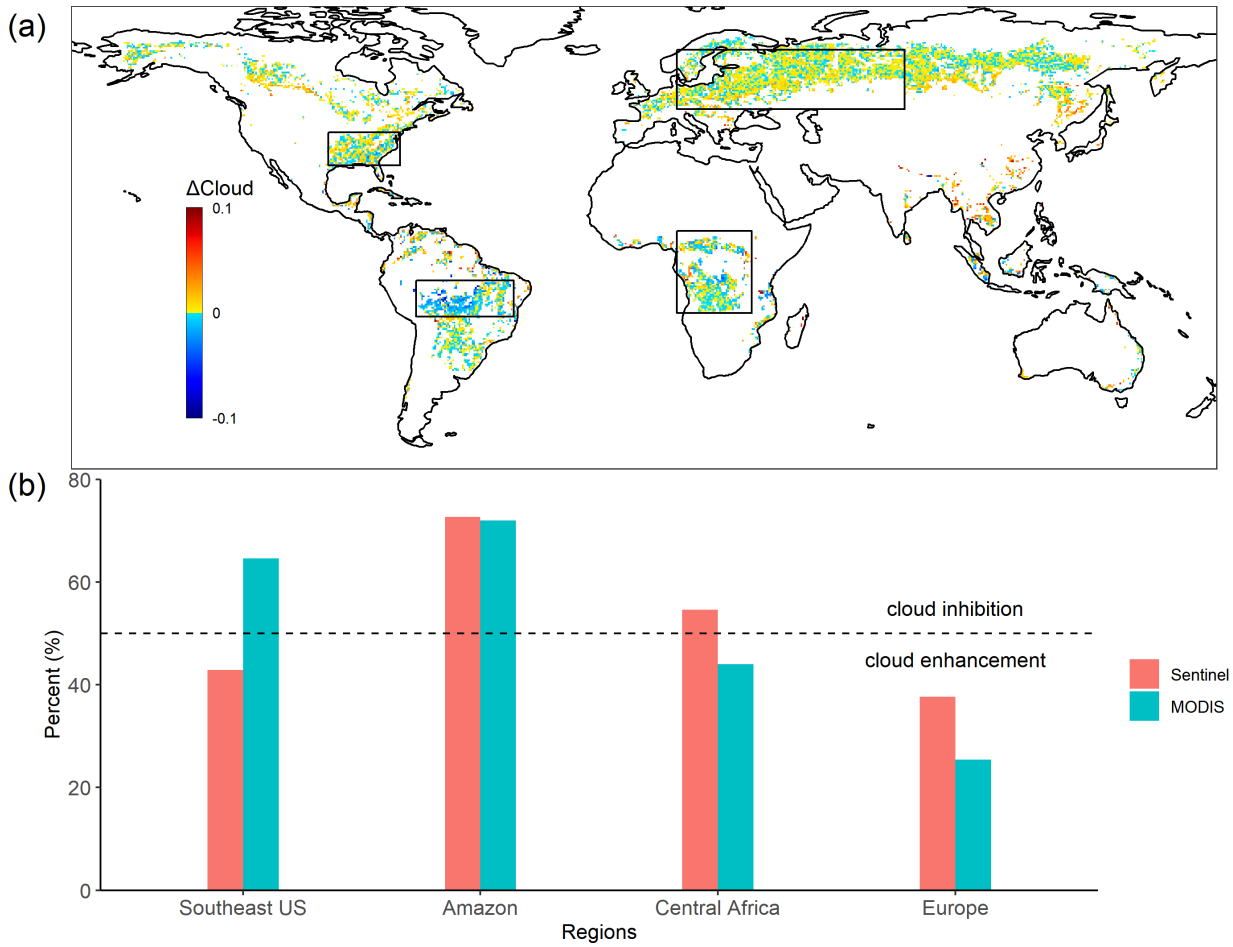

Figure S12. (a) The potential effect of forest on cloud cover based on Sentinel-5P data and (b) the percentage of negative ΔCloud in four selected regions between Sentinel-5P and MODIS. The four black rectangles in panel (a) denote four hotspots regions, Southeast US (lon: -97° to -75°; lat: 30° to 40°), Amazon (lon: -70° to -40°; lat: -16° to -5°), Central Africa (lon:10° to 33°; lat: -15° to 10°]) and Europe (lon: 10° to 80°; lat: 47° to 65°]. The dashed black horizontal line in panel (b) represents the 50% percent line, with value greater (less) than 50% indicating cloud inhibition (enhancement) of forest.

Table S1. Lookup table of converting CLM land classification scheme to IGBP scheme

CLM scheme*	IGBP scheme
4,5	broadleaf evergreen forest
6,7,8	broadleaf deciduous forest
1,2	needleleaf evergreen forest
3	needleleaf deciduous forest
1-8	mixed forest
1-11	savannas
9-11	shrubland
12-14	grass
15	crop

*CLM land classification scheme: 1 needleleaf evergreen temperate tree, 2 needleleaf evergreen boreal tree, 3 needleleaf deciduous boreal tree, 4 broadleaf evergreen tropical tree, 5 broadleaf evergreen temperate tree, 6 broadleaf deciduous tropical tree, 7 broadleaf deciduous temperate tree, 8 broadleaf deciduous boreal tree, 9 broadleaf evergreen temperate shrub, 10 broadleaf deciduous temperate shrub, 11 broadleaf deciduous boreal shrub, 12 arctic c3 grass, 13 cool c3 grass, 14 warm c4 grass, 15 crop

Table S2. Paired forest and nonforest flux sites used in this study

Pair number	Nonforest site	Forest site	Nonforest site latitude	Nonforest site longitude	Forest site latitude	Forest site longitude	Nonforest land cover
1	FR-Gri	FR-Fon	48.8442	1.9519	48.4764	2.7801	Cropland
2	NL-Hor	NL-Loo	52.2404	5.0713	52.1666	5.7436	Grassland
3	DE-Gri	DE-Tha	50.9495	13.5125	50.9636	13.5669	Grassland
4	DE-Kli	DE-Tha	50.8929	13.5225	50.9636	13.5669	Grassland
5	CA-NS6	CA-NS2	55.9167	-98.9644	55.9058	-98.5247	Open Shrubland
6	CA-NS6	CA-NS5	55.9167	-98.9644	55.8631	-98.485	Open Shrubland
7	CA-NS6	CA-NS1	55.9167	-98.9644	55.8792	-98.4839	Open Shrubland
8	CA-NS6	CA-NS3	55.9167	-98.9644	55.9117	-98.3822	Open Shrubland
9	CA-SF3	CA-SF1	54.0916	-106.005	54.485	-105.818	Open Shrubland
10	CA-SF3	CA-SF2	54.0916	-106.005	54.2539	-105.878	Open Shrubland
11	BE-Lon	BE-Vie	50.5515	4.7461	50.305	5.998	Cropland
12	US-Wi6	US-Wi0	46.6249	-91.2982	46.6188	-91.0814	Open Shrubland
13	US-Wi6	US-Wi3	46.6249	-91.2982	46.6347	-91.0987	Open Shrubland
14	US-Wi6	US-Wi4	46.6249	-91.2982	46.7393	-	Open

						91.1663	Shrubland
15	AU-Rig	AU-Whr	-36.6499	145.5759	-36.6732	145.0294	Grassland
16	IT-CA2	IT-CA1	42.3772	12.026	42.3772	12.026	Cropland
17	IT-CA2	IT-CA3	42.3772	12.026	42.38	12.0222	Cropland
18	DE-RuS	BE-Vie	50.8659	6.4472	50.3051	5.9981	Cropland
19	CZ-BK2	CZ-BK1	49.4944	18.5429	49.5021	18.5369	Grassland
20	US-Var	US-Blo	38.4133	-120.951	38.8953	-120.633	Grassland
21	IT-CA2	IT-Ro2	42.3772	12.026	42.3903	11.9209	Cropland
22	AT-Neu	IT-Ren	47.1167	11.3175	46.5869	11.4337	Grassland
23	DE-Kli	DE-Obe	50.8929	13.5225	50.7836	13.7196	Cropland
24	DE-Gri	DE-Obe	50.9495	13.5125	50.7836	13.7196	Grassland
25	US-Dk1	US-Dk2	35.9712	-79.0934	35.9736	-79.1004	Grassland
26	US-Dk1	US-Dk3	35.9712	-79.0934	35.9782	-79.0942	Grassland
27	US-NC1	US-NC2	35.8118	-76.7119	35.803	-76.6685	Open Shrubland
28	US-Fwf	US-Fmf	35.4435	-111.772	35.1426	-111.727	Grassland
29	STM_K77	STM_K83	-3.0202	-54.8885	-3.017	-54.9707	Cropland
30	RON_FNS	RON_RJA	-10.7618	-62.3572	-10.078	-61.9331	Pasture

Table S3. Parameter sets of window searching strategy for cloud cover data with different spatial resolutions. Parameters include raw data resolution (RawRes), window size (WinSize), window distance (WinDist), resolution for display (DisRes), and percent of negative ΔCloud. There are two parameter combinations for each resolution. The percentage of negative ΔCloud for different resolutions was calculated based on Fig. S11, without excluding areas with complex topography

RawRes	WinSize	WinDist	DispRes	Negative ΔCloud percent (%)
0.05°	9	5	0.5°	36.57
0.1°	9	5	0.5°	35.44
	5	3		35.75
0.25°	9	5	1.25°	30.50
	5	3		32.70
0.5°	9	5	2.5°	27.90
	5	3		29.45
1°	9	5	5°	24.36
	5	3		28.29